Title:

Hippocampal single-cell RNA Atlas of chronic methamphetamine abuse-induced cognitive decline in mice.

Authors and Affiliations

H Qiu, X Yue, YB Huang, ZL Meng, JH Wang* and DF Qiao*

H Qiu, Ph.D., School of Forensic Medicine, Southern Medical University.

X Yue, Ph.D., School of Forensic Medicine, Southern Medical University.

YB Huang, M.D., School of Forensic Medicine, Southern Medical University.

ZL Meng, M.D.,School of Forensic Medicine, Southern Medical University.

JH Wang*, Ph.D., Cancer Research Institute, School of Basic Medical Sciences, Southern Medical University, Guangzhou 510515, People' s Republic of China. E-mail address: wjh1987@smu.edu.cn.

DF Qiao*, Ph.D., School of Forensic Medicine,Southern Medical University, Guangzhou Key Laboratory of Forensic Multi-Omics for Precision Identification, Guangzhou 510515, Guangdong province, People' s Republic of China. E-mail address: qiaodf@smu.edu.cn.

*DF Qiao and JH Wang are Corresponding Authors.

Abstract

Background: Chronic methamphetamine abuse leads to cognitive decline, posing a significant threat to human health and contributing to productivity loss. However, the intricate and multifaceted mechanisms underlying methamphetamine-induced neurotoxicity have impeded the development of effective therapeutic interventions.

Methods: To establish a mouse model of cognitive decline induced by chronic methamphetamine exposure, we employed a large sample size and conducted two behavioral tests (Y-maze and novel object recognition test) at 2 and 4 weeks post-exposure. Subsequently, single-cell RNA sequencing was utilized to delineate the mRNA expression profiles of individual cells within the hippocampus. Comprehensive bioinformatics analyses, including cell clustering and identification, differential gene expression analysis, cellular communication analysis, pseudotemporal trajectory analysis, and transcription factor regulation analysis, were performed to elucidate the cellular-level changes in mRNA profiles caused by chronic methamphetamine exposure.

Results: Our findings demonstrated impairments in working memory, spatial cognition, learning, and cognitive memory. Through single-cell RNA sequencing, we identified diverse cell types in the hippocampi of mice after 4 weeks of behavioral testing, including neuroglial cells, stromal cells, vascular cells, and immune cells. We observed that methamphetamine exerted cell-specific effects on gene expression changes associated with neuroinflammation, blood-brain barrier disruption, neuronal support dysfunction, and immune dysregulation. Furthermore, cross-talk analysis revealed extensive alterations in cellular communication patterns and signal changes within the hippocampal microenvironment induced by methamphetamine exposure. Pseudotime analysis predicted hippocampal neurogenesis disorders and identified key regulatory genes implicated in chronic methamphetamine abuse. Transcription factor analysis uncovered regulators and pathways linked to astrocyte-mediated neuroinflammation, endothelial junction integrity, microglial synaptic remodeling, and

oligodendrocyte-supported neuronal cell bodies and axons. Additionally, it highlighted the role of neural precursor cells in various forms of neurodegeneration.

Conclusions: This study establishes a robust mouse model of cognitive impairment induced by chronic methamphetamine exposure. It provides valuable biological insights, characterizes the single-cell atlas of the hippocampus, and offers novel directions for investigating neurological damage associated with chronic methamphetamine-induced cognitive decline.

Keywords

Chronic methamphetamine abuse; Cognitive decline; Hippocampus; Single-cell RNA sequencing; Atlas

Introduction

Methamphetamine (METH), a widely abused psychostimulant globally, particularly in southeast and east Asia, currently holds the position of being the world's foremost illicitly manufactured synthetic drug. Its detrimental impact on human health, social stability, and economic development is immense(1). METH induces intense euphoria and addiction while causing significant harm to various tissues and organs, especially the central nervous system. With advancements in productivity and medical standards, research focusing on neuropsychiatric issues associated with chronic METH abuse has become a prominent topic concerning drug users' treatment, recovery, and quality of life. Chronic and regular usage of METH has been proven to result in an array of brain structural abnormalities such as cortical and hippocampal atrophy, nucleus accumbens hypertrophy, as well as decreased gray matter(2-4), leading to neuropsychiatric disorders including neurodegeneration, cognitive deficits, agitation, paranoia, depression, delusions, and schizophrenia. However, due to the wide range of affected targets and complex mechanisms underlying METH's effects,

the evolution and interplay during chronic processes make it challenging to analyze the etiology behind these neuropsychiatric diseases.

Extensive clinical and experimental evidences suggest that chronic METH abuse leads to cognitive deficits(5-7), which share similarities with neurodegenerative disorders such as impaired inhibitory control, learning and memory decline, attention decrease, increased pathological protein levels, neurotoxicity, neuroinflammation, and blood-brain barrier (BBB) injury. The hippocampus plays a crucial role in regulating cognitive functions as part of the limbic system. Previous studies have demonstrated that METH exerts complex negative effects on the hippocampus beyond its direct impact on dopaminergic and glutamatergic systems(8). It also indirectly affects various cell types within the hippocampus and alters the microenvironment. However, due to the intricate composition of the hippocampus and diverse mechanisms underlying METH's effects, certain impacts on vulnerable cell types and critical signaling pathways may be concealed during chronic exposure, making it challenging to unravel these mechanisms. Currently, there is limited understanding of the specific mechanisms responsible for chronic METH-induced neurotoxicity in the hippocampus leading to cognitive deficits; furthermore, theories explaining this wide range of effects are scarce.

In this study, we employed single-cell RNA sequencing (scRNA-seq) to construct a comprehensive hippocampal atlas of chronic METH abuse-induced cognitive decline in mice. To elucidate the underlying mechanisms by which chronic METH abuse affects the hippocampus and leads to cognitive deficits, we conducted animal behavior tests, performed scRNA-seq analysis with clustering and differential gene expression analyses, investigated cellular cross-talk, examined single-cell trajectories, and analyzed transcription factors. This study provides in vivo evidence of heterogeneous changes in hippocampal cells under chronic METH abuse and contributes to a more robust understanding of the mechanistic basis for cognitive deficits while also bridging previous theories on METH neurotoxicity.

Materials and methods

Animal and Treatments

All mice used were male and on C57BL/6 background. Healthy 7-week-old mice were purchased from Laboratory Animal Center of Southern Medical University (Guangzhou, China). Mice were quarantined for 2 weeks and then housed in Central Exhaust Ventilation Cage System (Houhuang experimental equipment technology, Suzhou, China) with 12 hours (h) light/12 h dark cycle in a temperature- (20–22 °C) and humidity- (45–55%) controlled vivarium and had ad libitum access to water and food. All protocols approved by the Institutional Animal Care and Use Committee in Southern Medical University (Ethical number: L2022125), and consistent with NIH Guidelines for the Care and Use of Laboratory Animals (8th Edition, U.S. National Research Council, 2011). After 1 week for adapting, mice were 10 weeks of age at the start of the experiment. They were randomly divided into two groups, and then treated by saline or methamphetamine (METH, National Institutes for the Control of Pharmaceutical and Biological Products, Beijing, China). Mice of METH group were administered METH dissolved in saline intra-peritonelly at a incremental dose from 1 up to 10mg/kg, and the daily dose was evenly divided into two doses at 12-hour intervals, while those of saline control underwent the same way of injection with saline simultaneously. The treatments lasted for 28 days. However the last administration of 12h before animal behevior tests or sample-collecting would be skipped. For scRNA-seq, we used 20 mice (10 from saline group, 10 from METH group, and each random 2 mice from same cage were composed of 1 sample).

Behavioral Experiments

Behavioral testing of mice used for scRNA-seq experiments followed an established protocol. To minimize any sitimulation, mice would be handled for 5 days to be habituated to environment and tester (30min to enviroment, 5min to tester)

before behavioral experiments. Less irritating behavioral experiments were used to evaluate in order to minimize impacts on scRNA-seq.

Y-Maze

Y maze test was used to evaluated spontaneous alternation behavior in mice. The Y-maze was made of three arms set at angles of 120°. It's walls are covered with frosted adhesive paper. Mice were placed in the end of fixed arm of y-maze, then they were allowed to freely explore whole y-maze for 8-min session while camera system recorded the behavior of mice. The total number of entries of each arms (recognizing that all four legs of mouse entered the arm as the standard for entries), the number of alternations (an alternation is defined as successive entries into the three arms on overlapping triplet sets.) and the ratio of them were regarded as statistical indicators to assess spatial working memory.

Novel Object Recognition Test

Novel object recognition test (NOR) was applied to assess mice recognition memory. The testing room was lit with four LED lights which provide the light intensity of approximately 20 lx in each test box (50 × 50 × 40 cm). Mice were put into test room to habituate for 24h before begining of test, and would be given 10 min to explore the object-free box and were then returned to their home cage. In training stage, two objects of same appearance were placed at a symmetrical position in test box where mice would explore freely for 10min to be fully acquainted with objects. After training, mice were sent back to their home cage to rest for 30min. Then in testing stage, they were placed back into original test box with a familiar old object and a novel one at the same place and also allowed to explore freely for 10min. The familiar object and novel object and their placement were counterbalanced within each group. Camera system was placed above the test box and recorded behaviors of mice in test box for statistics.

The following behaviors were scored as exploration: biting, sniffing, licking, touching the object with the nose or with the front legs, or proximity (≤1 cm) between the nose and the object. If the mouse put its hind legs on objects, or standed on top of the object or completely immobile, exploration was not scored. The preference index for the novel object was calculated as (time spent exploring the new object/the total time spent exploring both objects), and the discrimination index was calculated as (time spent exploring the new object − time spent exploring the familiar old object) / (total time spent exploring both objects). Behavior was scored on video by two observers blinded to the mice's treatment.

Brain Samples Collecting

For scRNA-seq, we used hippocampus tissues of 20 mice (10 from saline group, 10 from METH group, and each random 2 mice from same cage were regarded as 1 sample). Hippocampus collecting was carried out under the guidance of JOVE(8). Whole hippocampus was dissected integrally on icein the shortest time (within 5min) and preserved in tissue preservation solution (SeekGene, China) at 4℃for following tissue dissociation.

Cell Preparation for Sing Cell RNA Sequencing

After harvested, tissues were washed in ice-cold RPMI1640 and dissociated using Tissue Dissociation Reagent A (Seekone K01301-30, China) from SeekGene as instructions. DNase Ⅰ(Sigma 9003-98-9, USA) treatment was optional according to the viscosity of the homogenate. Cell count and viability was estimated using fluorescence Cell Analyzer (Countstar® Rigel S2) with AO/PI reagent after removal erythrocytes (Solarbio R1010, China) and then debris and dead cells removal was decided to be performed or not (Miltenyi Biotec 130-109-398/130-090-101, USA). Finally fresh cells were washed twice in the RPMI1640 and then resuspended at 1×10^6 cells per ml in 1×PBS and 0.04% bovine serum albumin.

Single Cell RNA Sequencing Library Construction and Sequencing

Single-cell RNA-Seq libraries were prepared using Chromium Next GEM Single Cell 3' Reagent Kits v3.1 (10x Genomics Catalog No.1000268, USA). Briefly, appropriate number of cells were mixed with reverse transcription reagent and then loaded to the sample well in Chromium Next GEM Chip G. Subsequently Gel Beads and Partitioning Oil were dispensed into corresponding wells separately in chip. After emulsion droplet generation reverse transcription were performed at 53℃for 45 minutes and inactivated at 85℃for 5 minutes. Next, cDNA was purified from broken droplet and amplified in PCR reaction. The amplified cDNA product was then cleaned, fragmented, end repaired, A-tailed and ligated to sequencing adaptor. Finally, the indexed PCR were performed to amplified the DNA representing 3’ polyA part of expressing genes which also contained Cell Bar code and Unique Molecular Index. The indexed sequencing libraries were cleanup with SPRI beads, quantified by quantitative PCR (KAPA Biosystems KK4824) and then sequenced on illumina NovaSeq 6000 with PE150 read length.

Processing the Single Cell RNA Sequencing Data and Date Quality Control

The raw sequencing data was precessed by Fastp firstly (Chen, Zhou et al. 2018) to trim primer sequence and low quality bases. And then we employed the Cell Ranger software v7.0 (10X Genomics) obtained from https://www.10xgenomics.com/support/software/cell-ranger/downloads to precess sequence data and aligned to mouse mm10 genome in order to obtain gene expression matrix. Subsequently, the gene expression matrices of each sample were obtained and further analyzed using Seurat v.4.4.0. Then we determined effective cells using the following criteria: (a) total UMI counts more than 1,000 but less than the 97th percentile for each cell; (b) gene numbers between 1000 and 7,000; (c) percentage of mitochondrial genes <10%; and (d) percentage of hemoglobin genes < 0.1%. Moreover, We excluded genes expressed in fewer than 3 cells, as well as

MALAT1, mitochondrial genes, and hemoglobin genes. And the remaining cells and genes were used for subsequent analysis. Quality control charts are included in SI.4.

Data integration, Dimensionality reduction, and Clustering

After performing quality control and filtering, DoubletFinder v2.0.3 was then employed to identify double cells with an expectation value of doublets was calculated as an increase of 0.8% for every 1,000 additional cells, pN at 0.25, and pK according to function Find.pk. Library-size normalization was conducted for each cell using the NormalizeData function in Seurat v.4.4.0. The 2,000 most variable genes were identified using the FindVariableGenes. Subsequently, all libraries were integrated using Harmony (Ilya Korsunsky et al., 2019) to correct batch effects. ScaleData was applied to regress out variability associated with the numbers of UMIs, followed by dimensionality reduction through RunPCA and RunUMAP (dimensions=1:20). Finally, clustering of cells was performed using the FindClusters function with a resolution of 0.8 based on the 1: 24 dimensions.

Celltype Identifcation

FindAllMarkers was used to compare each cluster to all others to identify canonical cell type -specific marker genes. Each retained marker gene was expressed in a minimum of 25% of cells and at a minimum log fold change threshold of 0.25. The clustering differential expressed genes were considered significant if the adjusted P-value was less than 0.05 the avg_log2FC was ≥ 0.25. And the cluster were annotated using cell type-specific signatures and marker genes from Cellmarker2.0 and PanglaoDB.

Differentially Expressed Genes (DEGs) analysis and Enrichment Analysis

DEG analysis between cell types was performed following the muscat (v.1.16.0, Crowell et al. 2020) R package pipeline, which facilitates multi-sample, multi-condition

comparisons of single-cell RNA-seq data. Genes were ranked by absolute log2 fold-change (log2FC), and those with p-values>0.05 (adjusted for multiple comparisons) and log2FC<0.25 were removed. Gene Ontology (GO, https://www.geneontology.org/) enrichment analysis of DEGs was implemented by the clusterProfiler R package (Yu et al., 2012). GO terms with corrected Pvalue less than 0.05 were considered significantly enriched by DEGs. Kyoto Encyclopedia of Genes and Genomes database (KEGG, http://www.genome.jp/kegg/, Kanehisa et al., 2008) is a database resource for understanding high-level functions and utilities of the biological system, such as the cell, the organism and the ecosystem, from molecular-level information, especially large-scale molecular datasets generated by genome sequencing and other high-through put experimental technologies. We used clusterProfiler R package to test the statistical enrichment of DEGs in KEGG pathways.

Cellular Cross-talk Analysis

We used the Cellchat (v.1.6.1, Suoqin Jin et al., 2021, http://www.cellchat.org/) to analyze the expression abundance of ligand–receptor interactions among hippocampal cell types. We followed the guidelines of Cellchat as reference(9). Cell communication networks were inferred by identifying differentially expressed ligands and receptors between the different hippocampal cell types. The probabilities of these interactions on the ligand-receptor level were computed using the default 'truncatedMean' method setting the average expression of a signaling gene to zero if it is expressed in less than 10% of the cells in one group. The effect of population size was corrected when calculating the interaction probabilities. In addition, the L-R interaction probabilities within each signaling pathway were summarized to compute pathway-level communication probabilities by the function 'computeCommunProbPathway'. Cell–cell communication networks were then aggregated by summing the number of links or the previously calculated communication probabilities by the function 'aggregateNet'. To compare the signaling patterns between METH and Saline groups, we performed differential expression

analysis between all the METH versus Saline groups in each cell types. To better control the node size and edge weights of the inferred network across different datasets, we calculated the maximum number of cells per cell group and the maximum number of interactions (or interaction weights) across two datasets. We recognized differental and conservative networks by their functions and calculated their divergence indicators. We also compared outgoing (or incoming, or all) signal patterns between two data sets and different celltype. To dentificated of major signaling roles of cell types in specific pathways, we visualize the computed centrality scores using heatmap. Discrepant ligands and receptors were identified if each had a log-fold change (logFC) and a percent of cells expressed in one cluster both above 0.1 in the senders and receivers by the function ‘identifyOverExpressedGenes’, respectively. Then, we extracted the differentially expressed L-R pairs as those with upregulated or downregulated ligands and receptors in the METH compared to Saline groups.

Pseudotime analysis

Monocle2(10) (version 2.18.0) was employed for pseudotime trajectory analysis to elucidate the differentiation trajectory of cell development. The UMI matrix was extracted from the Seurat object and used to create a new object with the newCellDataSet function. For the trajectory analysis, 2000 highly variable genes were selected, followed by dimensionality reduction using the DDRTree method and cell ordering with the orderCells function. Differential genes along the pseudotime trajectory were identified using the differentialGeneTest function. The plot_cell_trajectory function was utilized to visualize the trajectory in a two-dimensional space, effectively presenting the cell differentiation state. The branches observed in the single-cell trajectories represent varying biological functions, which are inferred from gene expression patterns during development.

SCENIC analysis

SCENIC analysis was utilized to explore key transcription factors (TFs) regulating differences across cell types. The analysis was conducted using pySCENIC with default parameters, following the established protocol(11). Initially, A co-expression network was constructed using grnboost2. Subsequently, regulons for each transcription factor were inferred using the RcisTarget motif databases(12) (mm10-refseq-r80-10kb-up-and-down-tss.mc9nr.feather and mm10-refseq-r80-500bp-up-and-100bp-down-tss.mc9nr.feather). Activity scores (AUC) for each TF regulon in individual cells were calculated using AUCell. Significant TF regulons associated with specific cell types were identified using the FindAllMarkers function in Seurat. The regulatory networks involving transcription factors and their target genes were further analyzed using Cytoscape (v3.10.1). Additionally, enrichment analyses of target genes were performed using the clusterProfiler R package, as mentioned previously.

Statistical Analysis

For the experimental data, we used GraphPad Prism software (version 8.0.2, USA) to perform statistical analyses and graphic plotting. We checked normal distribution of data using the Shapiro–Wilk test, though our sample size was close to 30 as a large sample in each group. The Y maze and NOR test datas were expressed as mean ± SEM. We used Unpaired Student's t test to analyze the between-group differences in alternation triplet of Y maze, and discriminant index, preference index, total time and frequence spent on explorations on new and old objects in 10min. The P value <0.05 was considered statistically significant. All statistical tests were two-tailed. For the single-cell RNA sequencing data, we used R v4.3.1 for the statistical analyses and graphic generation. Bioinformatic tools were used to analyze cellular clustering, differentially expressed genes, enrichment cross-talk, single-cell trajectory and SCENIC analysis.

Result

1. Chronic METH exposure led to cognitive decline in adult mice.

METH chronic exposure mouse model construction and behavioral experiment arrangement is shown in the Fig.1.A. Adult male mice subjected to chronic METH exposure exhibited significant declines in working memory and spatial cognition, as demonstrated by Y-maze tests conducted at the end of both the second and fourth weeks of administration. The mean differences between METH-treated (n=32) and saline-treated (n=29) groups were -0.1664(95%CI:-0.2126 to -0.1202, p<0.0001) for the 2-week test, and -0.2202(METH (n=30) vs. Saline (n=29), 95% confidence interval (CI):-0.2728 to -0.1676, p<0.0001) for the 4-week test (Fig.1.B).

After chronic METH abuse, NOR tests also revealed impairments in the ability of animals to discriminate novel objects. In 2-week NOR test, the discrimination index for saline-treated mice (n=29) was 0.3119±0.0300 (mean±SEM), whereas for METH-treated mice (n=29) was 0.1569±0.0462. The mean difference in discrimination index between METH and Saline groups was -0.1550±0.0551, p=0.0068, 95% CI:-0.2653 to -0.0446 (Fig.1.C). The preference index for saline-treated mice was 0.6559±0.0150, while for METH-treated mice it was 0.5785±0.0231, tresulting in a mean difference between METH and Saline of -0.07748±0.0276, p=0.0068, 95% CI:-0.1327 to -0.0223 (Fig.1.C). Total exploration time for novel objects by saline-treated mice was measured at 28.36±2.285, compared to 18.38±1.453 observed among METH treated mice. The mean difference in total exploration time of the novel object was estimated as -9.974±2.708, p=0.0005. Similarly total exploration time spent on old objects by saline group amounted to 14.79±1.173, versus 13.44±1.067 recorded among their counterparts receiving METH treatment. The mean difference in total exploration time of the old object was estimated as -1.352±1.586, p=0.3976 (Fig.1.D). Exploration frequency analysis showed that the number of times novel object were explored by saline group averaged 25.55±1.565, as opposed 19.66±1.368 seen among those exposed to

METH. The mean difference in exploration frequency of the novel object was estimated as -5.897±2.079, p=0.0063 (Fig.1.E). Furthermore,the exploration frequency associated with old object within saline group stood at 19.14±1.359 relative 15.41±1.010 noted within Methamphetamine treated subjects. The mean difference in exploration frequency of the old object was estimated as -3.724±1.693, p=0.0320 (Fig.1.E). Our findings suggest that following a 2-week METH treatment, there was a significant decline observed in the cognitive and mnemonic abilities as well as exploratory behavior of mice.

In the 4-week NOR test, the discrimination index of saline (n=29) was 0.3019±0.0389, while discrimination index of METH (n=29) was 0.0880±0.0368. The mean difference in discrimination index between METH and Saline groups was calculated as -0.2139±0.0536, p=0.0002, 95% CI:-0.3213 to -0.1066 (Fig.1.F). The preference index for saline administration was measured at 0.6510±0.0195, whereas that for METH administration yielded a value of 0.5440±0.0184. The mean difference in preference index between METH and Saline groups was estimated as -0.1070±0.0268, p=0.0002, 95% CI:-0.1606 to -0.0533 (Fig.1.F). The total exploration time of the novel object in the saline group was 20.04±1.502, whereas it was 13.05±1.019 in the METH group. The mean difference in total exploration time of the novel object was estimated as -6.996±1.815, p=0.0003 (Fig.1.G). Total exploration time of old object of saline was 10.50±0.919, while that of METH was 11.39±1.119, The mean difference in total exploration time of the old object was estimated as 0.8922±1.448, p=0.5402 (Fig.1.G). Exploration frequency of novel object in saline group was 22.10±1.293, and that in METH was 18.52±1.521. The mean difference in exploration frequency of the novel object was estimated as -3.586±1.996, p=0.0778 (Fig.1.H). Exploration frequency of old object in saline group was 18.10±1.658, and that in METH was 15.03±1.585, The mean difference in exploration frequency of the old object was estimated as -3.069±2.294, p=0.1864 (Fig.1.H). These findings demonstrate that chronic METH abuse induces a decline in learning and cognitive memory abilities in mice. Although there were no differences observed in exploration frequency between the METH and saline groups during the 4-week test, the

discrimination and preference indexes exhibited greater statistical significance and further declined in the METH group compared to those observed during the 2-week test. These results suggest that prolonged METH use may progressively impair cognitive function.

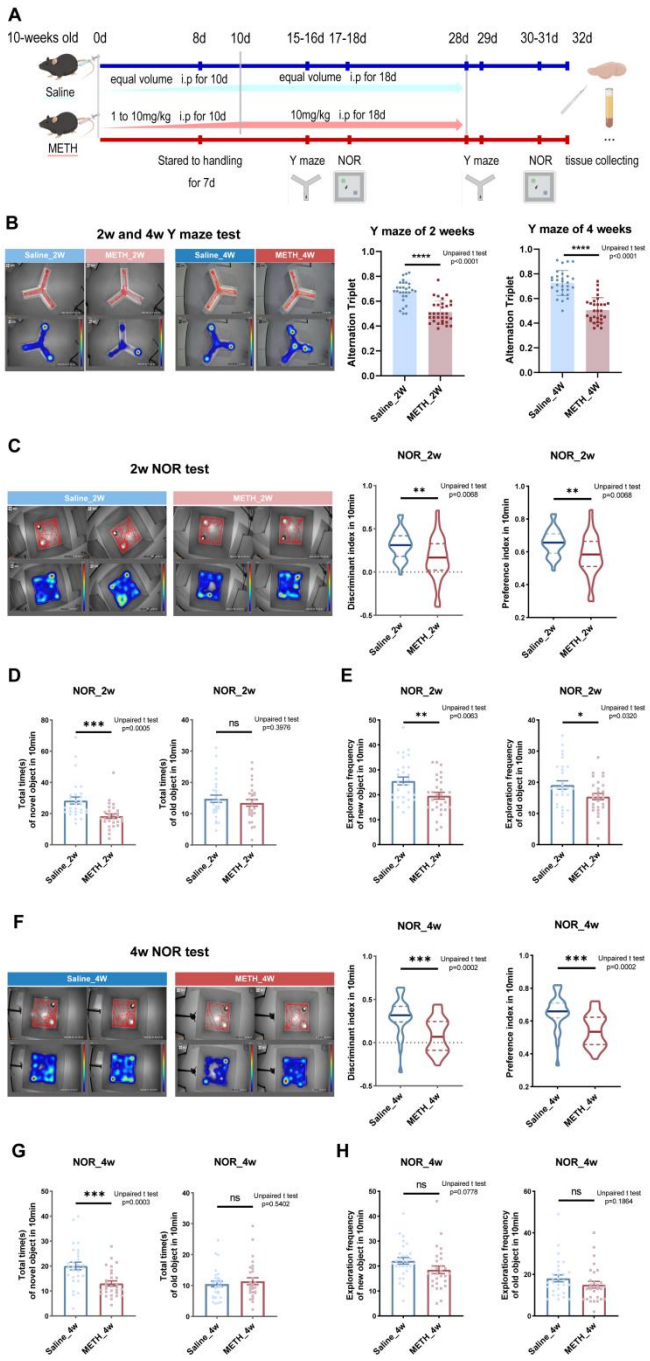

Fig.1. Mice treatment and result of behaviour tests. (A) The construction mouse model of chronic methamphetamine abuse. (B) The track visualizations and heatmaps of Y maze in 2 and 4 weeks. (C)

The track visualizations, heatmaps and the discrimination and preference index of 2 weeks NOR test. (D-E) The total exploration time and frequency of familiar or novel objects of 2 weeks NOR test. (F) The track visualizations, heatmaps and the discrimination and preference index of 4 weeks NOR test. (G-H) The total exploration time and frequency of familiar or novel objects of 4 weeks NOR test. Asterisks indicate statistical significance (*$p < 0.05$; **$p < 0.01$; ***$p < 0.001$; ****$p < 0.0001$). All data are presented as mean ± SEM.

2. Identification of hippocampal cell clusters in mice with chronic METH exposure.

To investigate the impact of chronic METH abuse, single-cell RNA-seq was conducted on the hippocampi of mice treated with saline or METH. A total of 60,549 high-quality cells were captured after stringent filtration, comprising 31,219 cells from saline-treated mice and 29,330 cells from METH-treated mice. The samples were then subjected to clustering analysis based on their gene expression profiles using cluster-specific variable gene signatures, following the Seurat pipeline (logfc.threshold = 0.25, min.pct = 0.25). Subsequently, Uniform Manifold Approximation and Projection (UMAP) analysis at a resolution of 0.8 revealed a total of 31 distinct transcriptional clusters in each experimental group (Fig.2.A). By leveraging established hippocampal markers from databases (primarily Cellmarker2.0 and PanglaoDB), we identified 18 distinct cellular components within the hippocampus, including astrocytes (cluster6 and 27, with *Aqp4*, *Gfap*, *Gja1* and *Slc1a3* as markers), cajal-Retzius cells (cluster14, with *Cntnap2*, *Reln*, *Clstn2* and *Kcnh7* as markers), *Cldn5*$^{+}$ *and Cldn5*$^{-}$ mural cells (cluster9 and 11, with *Vtn*, *Pdgfrb*, *Rgs5* and *Atp13a5* as markers, and distinguished by high or low expression of *Cldn5*), endothelia (cluster4, 7, 8, 10 and 16, with *Cldn5*, *Flt1*, *Pecam1* and *Kdr* as markers), ependymal cells (cluster23, with *Ccdc153*, *Tmem212*, *Rarres2* and *Mia* as markers), fibroblasts (cluster25, with *Dcn*, *Spp1*, *Nupr1* and *Igfbp2* as markers), macrophage (cluster12, with *Pf4*, *Mrc1*, *F13a1* and *Lyz2* as markers), microglial (cluster0,1,3,21 and 29, with *Tmem119*, *Cx3cr1*, *P2ry12* and *Aif1* as markers), neurons or neuroblasts (cluster17, with *Igfbpl1*, *Sox11*, *Fabp7*

and *Nnat* as markers), neutrophils (cluster26, with *S100a9*, *Retnlg G0s2* and *Slpi* as markers), NK-T cells (cluster19, with *Ccl5*, *Trbc2*, *Cd3g* and *Ms4a4b* as markers), neural stem cells (NSC, cluster20, with *Clu*, *Aldoc*, *Cpe* and *Hopx* as markers), neurons from NSC (cluster22, with *Chchd10*, *Pcp4*, *Fxyd1* and *Ppp1r1b* as markers), oligodendrocytes (cluster2,5,24,28 and 30, with *Mbp*, *Mog*, *Cldn11* and *Mag* as markers, and cluster24 are called perivascular oligodendrocyte), oligodendrocyte precursor cells (cluster13, with *Pdgfra*, *Cacng4*, *Sox10* and *Cspg4* as markers), smooth muscle cells (cluster15, with *Acta2*, *Myl9*, *Tagln* and *Myh11* as markers), and T cells (cluster18, with *Cd44*, *Cd52*, *Cd74* and *Plac8* as markers). The top 4 highly expressed genes of each cluster were exhibited (Fig.2.B and D, SI.1). These findings suggest that besides neurons, hippocampus is composed of a rich diversity of cell types including neuroglias, stroma cell, vascular cells and immune cells, thereby constituting a complex yet organized microenvironment. Within this microenvironment, METH can exert broad effects on various cell types which may contribute to impairments in learning and memory. This knowledge could potentially unveil the characteristics and functional alterations of specific hippocampal cell types.

After conducting clustering analyses, the cell proportion analysis reveals that following chronic METH abuse, there was a decrease in the proportion of astrocytes from 6.6% to 5.5%, endothelial from 24.3% to 22.5%, smooth muscle cell from 1.0% to 0.6%, the proportion of oligodendrocyte precursor cell from 1.6% to 1.0%, neutrophils from 0.3% to 0.1%, ependymal cell from 0.4% to 0.3%, fibroblasts cell from 0.3% to 0.2%. Conversely, there was an increase in the proportion of microglial from 36.0% to 39.8%, NK-T cell from 0.5% to 0.7%, neuron from NSC from 0.2% to 0.6% (Fig.2.C).

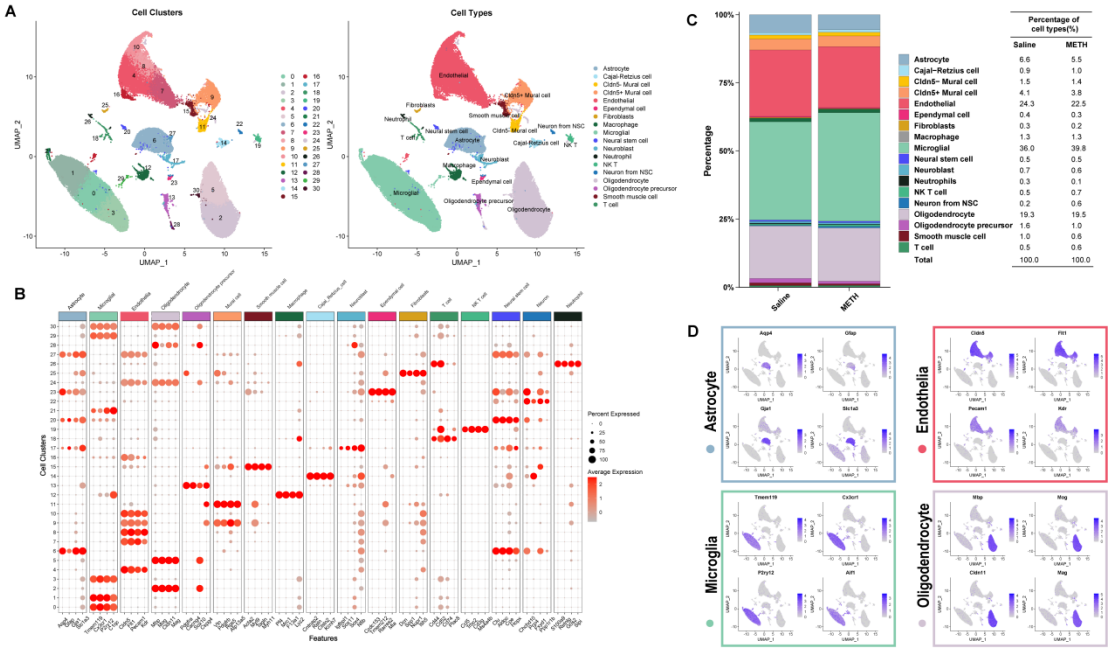

Fig.2. Hippocampus cell clusters of saline and METH mice. (A) The Umap-distributed plots showing 31 hippocampal cell clusters in saline and METH groups. (B) The average expression of known marker genes of hippocampal clusters. (C) The percentage of cells in hippocampal clusters in saline and METH groups. (D) The marker genes expression's featureplots of astrocyte, endothelia, microglia and oligodendrocyte.

3. Chronic METH exposure induced gene and function changes of hippocampal cells in mice.

Chronic METH abuse elicits a diverse array of cellular responses, ultimately resulting in multifactorial cognitive decline. To elucidate the underlying mechanisms of this cognitive impairment, we employed muscat, which utilizes a pseudobulk approach for multi-sample, multi-condition, cluster-specific differential gene expression analysis, to identify differentially expressed genes (DEGs) within each cell cluster. Remarkably, we observed that the majority of DEGs were unique to specific cell types following chronic METH exposure. For instance, Cldn5+ mural cells exhibited the highest number of DEGs with 679 identified (368 upregulated and 311 downregulated) (Fig.3.A), including 336 cell type-specific DEGs (Fig.3.B). Similarly,

endothelial cells displayed 565 DEGs (322 upregulated and 243 downregulated) (Fig.3.A), with 268 being cell type-specific. Notably, these two cell types shared a subset of 116 common DEGs (Fig.3.B).

Subsequently, these differentially expressed genes (DEGs) were segregated based on their up-down regulated relationship and subjected to individual pathway enrichment analysis severally using Gene Ontology (GO), aiming to elucidate the functional roles and underlying pathogenesis of cognitive decline. Up/down-regulated Biological Processes (BP) of GO were shown (Fig.3.C-F and SI.2). Furthermore, when examining cell type-specific enrichment patterns in chronic METH abuse-induced genes, we observed that functional annotations not only revealed specific effects but also intricate co-regulatory mechanisms across various cell types.

Neuroinflammation is a complex process that can be triggered by various factors, such as exposure to toxic substances like METH. METH-induced neuronopathies, in particular, have been found to constantly produce a range of impact factors and cells' changes that contribute to the exacerbation of neuroinflammation. Microglia up regulates immunoprotein receptor genes (such as *Fcer1g*, *Fcgr3* and *Il1rl2*) to enhance immune sigal reception and cell chemotaxis (*Ccl2*, *Cxcl14*, *Trpv4*, et al.) (Fig.3.E). Astrocyte improve abilities of gliogenesis and migration (*P2ry12*, *Rras*, *Efemp1*,et al.) to regulatie inflammatory response with NF-κB signal path (*Tnfaip6*, *Nfkb1*,*Nfkbia*) involving (Fig.3.C). Apart from reactions of neurogliocytes, *Grn*, *Trem2* (associated with astrocye and microglia activation) are up-regrated in both microglia and T cell, which indicates that central resident and peripheral immune cells may have communication and participate jointly in neuroinflammatory response. T and NK-T cells become more active in leukocyte or lymphocyte mediated immunity, but T cells active by complement-mediation (*C1qb*, *C1qc*, *C1qa*, *Trem2*) while NK-T cells depend more on reception of cytokines (*Il18r1*, *Fcer1g*) or recognition of receptors on membrane (*Itgb2*, *Ptprc*, *Tyrobp*,et al.). However neutrophils down-regulate chemokine-mediated signaling pathway (*Cxcr4*, *Ccl3*, *Ccl4*) that may indicates neuroinflammation changes from acute (leukocyte-leading) to chronic

(lymphocyte-leading). Macrophage also weaken leukocyte activation (*Cd28*, *Itgam*, *Il18*, *Tnfsf9*, et al.) but strengthen T cell activation.

The maintenance of a stable neural microenvironment relies on a healthy blood-brain barrier (BBB) system. METH can induce structure and function disruptions in the BBB, although its chronic effects remain uncertain. In our study, we observe that endothelial cells upregulate detoxification funtions (*Gstm1*, *Abcg2*, *Fbln5*, et al.) and autophagy-related genes (*Qsox1*, *Fnbp1l*, *Trp53inp1*, et al.), while downregulating angiogenesis-associated genes (*Hipk2*, *Tnfrsf1a*, *Vegfc*, *Cldn5*, et al.) and cell-cell adhesion molecules (*Hmcn1*, *Ceacam1*, *Cdh10*, et al.). Furthermore,endothelial dysfunction is also implicated in learning or memory deficits and cognitive impairments (*Dbi*, *Bche*, *Psen2*, *Prnp*, et al.) as well as nervous system development (*Macf1*, *Ptprz1*, *Vegfc*, *Ctnnb1*, et al.) suggesting an interplay between neuronal activities and vascular functions (Fig.3.D). Similarly,dysfunctions in *Cldn5*$^{+}$ mural cells are associated with altered vascular permeability (*Ctnnbip1*, *Pde3a*, *Ceacam1*, *Cldn5*) and developmental processes (*Atp2b4*, *Sfrp2*, *Vegfc*, *Tgfbr2*, et al.), as well as cognitive impairments (*Psen2*, *Bche*, *Nf1*, *Prkn*, et al.), and increased autophagic cell death (*Bmf*, *Bnip3*, *Lamp1*, *Cdkn2d*) after METH trearment. As a structure of arteriole in hippocampus, SMCs exhibit suppressed inflammatory responses such as leukocyte migration (*Abl2*, *Fcer1g*, *Vcam1*, *Icam1*, et al.), glial cell activation (*Syt11*, *C1qa*, *Cx3cr1*, *Trem2*, et al.) and IL-6 production (*Dhx9*, *Fcer1g*, *Syt11*, *Il6ra*).

The response of cell types in BBB to METH is heterogeneous. For instance, in the Wnt signaling pathway (whose active state improve angiogenesis and vascular remodeling), both *Cldn5*$^{+}$ and *Cldn5*$^{-}$ mural cells exhibit down-regulation by some different DEGs, while endothelial cells up-regulate it. Cell-substrate adhesion is strengthened in mural cells and SMCs, but weakened in ECs. Although this leads to an increase in BBB permeability, the underlying mechanisms vary across the inner and outer layers of blood vessels.

Metabolite shuttling and extracellular vesicle signaling provided by oligodendrocytes are essential for the normal functioning of neurons, particularly their axons(13). In our study, we observed significant changes in the metabolic status of oligodendrocytes (Fig.3.F), including alterations in organic acid biosynthesis (*Cyp27a1*, *Per2*, *Glul*, et al.), amino acid metabolic (*Glul*, *Bcat1*, *Hmgcll1*, et al.), glycolipid metabolic process (*Pikfyve*, *Pigc*, *Pnpla7*, et al.) and other processes. Additionally, METH influences neural structure and function-related changes such as axonogenesis (GO terms:axonogenesis, postsynapse organization, central nervous system neuron development, et al.) and synaptic vesicle signaling (GO terms: vesicle-mediated transport in synapse, synaptic vesicle recycling, vesicle localization, et al.), which are partially upregulated or downregulated. Furthermore, oligodendrocyte precursor cells exhibit negative effects on cell development and synaptic plasticity while also increasing neuroinflammation response to DNA damage stimulus. These effects may contribute to neuronal dysfunction and ultimately lead to cognitive decline. Astrocytes play a vital role in supporting neuronal function throughout the central nervous system by regulating synapse development and neurotransmitter release at synapses while providing adequate energy supply and modulating information processing within neurons(14). During chronic METH abuse, astrocytes downregulate bioprocesses involved in translation and metabolism (Fig.3.C), such as translation at synapse (*Rpl12*, *Rpl35*, *Rps26*, et al.) and the generation of precursor metabolites and energy (*Adh5*, *Ndufa5*, *Bpgm*, et al.), which may impede normal neurotransmitter vesicle transmission. Simultaneously, astrocytes enhance bioprocesses related to multiple inorganic cation transportation including potassium (*P2ry12*, *Kcnd3*, *Slc24a2*, et al.), sodium (*Slc24a2*, *Nkain1*, *Hcn2*, et al.), or calcium (*P2ry12*, *Tmem38a*, *Slc24a4*), which may interfere regulation of neural membrane potential. However, we also observe that astrocytes have positive effects of neuron projection extension (*Nrp2*, *Rtn4*, *Jade2*, et al.), axon ensheathment (*Abca2*, *Mal*, *Ugt8a*, et al.), or oligodendrocyte differentiation (*Abca2*, *Mal*, *Mag*, et al.). These results may imply that astroctyes have dfferent subsets performing diverse functions according to their positions and cellular contacts in hippocampus.

Adult hippocampal neurogenesis (AHN) is a complex developmental processes influenced by multiple factors, from NSC, radial glia-like cell, neuroblast to mature neuron, which are important in learning, memory and emotional regulation and linked to memory deficits due to this process can enhance the plasticity of the hippocampus. At the initiation of AHN, we observe that NSCs down-regulate generation of precursor metabolites and energy (*Sdhaf4*, *Nduf* family, *Uqcrh*, *Gapdh*, et al.) meaning that METH could impede cell proliferation and differentiation of NSCs. Additionally, METH arouses endoplasmic reticulum stress (*Tmco1*, *Atf3*, *Hspa5*, *Gsk3b*, et al.), apoptotic process (*Btg2*, *Prnp*, *Cebpb*, *Ctsz*, et al.) and autophagy (*Ddrgk1*, *Ctsa*, *Mcl1*, *Sh3glb1*, et al.) in NSCs, and therefore leads to increase of amyloid-beta (*Prnp*, *Apoe*, *Psenen*, *Rtn4*, et,al) or IL-6 (*Ncl*, *Fcer1g*, *Il1a*, *Lbp*, et al.) triggering neuroinflammation. neurogenesis (*Per2*, *Mag*, *Fbxo31*, et al.). Adult NSC activation in mice is regulated by circadian rhythms and intracellular calcium dynamics(15). In our data, astrocytes of METH-treated mice exhibit enhanced activity compared to saline-treated mice in terms of circadian rhythm-related genes (*Per2*, *Ptgds*, *Ciart*, *Id3*, et al.), calcium-mediated signaling (mentioned above), and regulation of neurogenesis (*Per2*, *Mag*, *Fbxo31*, *Slc7a5*, et al.). These findings suggest that astrocytes attempt to maintain the population of regenerated neurons by activating NSCs; however, this may lead to an earlier depletion of the NSC pool. During the neuroblast stage, METH induces increased oxidative stress in neuroblasts through upregulation of genes involved in oxidative stress response (*Setx*, *Prkra*, *Agap3*, *Lig1*, et al.) as well as alterations in DNA regulation related to cell division processes (*Ciz1*, *Rpa2*, *Mcm7*, *Ssbp1*, et al.). Additionally, METH weakens the adhesion between neuroblasts and their substrate through downregulation of genes associated with cell-substrate adhesion (*Myoc*, *Ccn1*, *Ptn*, *Lrp1*, et al.). With the gradual development of the remaining neuroblasts into neurons, METH exhibits stronger effects on neurons derived from NSCs, leading to a higher number of DEGs. Under the influence of METH, neurons from NSCs up-regulate their response to endoplasmic reticulum stress (*Tmco1*, *Atf3*, *Hspa5*, *Pdia3*, et al.), TNF superfamily cytokine production (*Ncl*, *Fcer1g*, *Il1a*, *Lbp*, et al.), neuron death (*Prnp*, *Ctsz*, *Mcl1*, *Jun*, et al.), leukocyte

chemotaxis (*Fcer1g*, *Lbp*, *Cxcl10*, *Hmgb1*, et al.) and amyloid-beta metabolic process (*Prnp*, *Apoe*, *Psenen*, *Rtn4*, et,al). Meanwhile neurons from NSCs down-regulate a series of energy metabolic process (*Sdhaf4*, *Nduf* family, *Cycs*, *Gapdh*, et al.) and structure and function of mitochondria-relating process (*Slc25a* family, *Vdac1*, *Atpif1*, *Acaa2*, et al.). Cajal-Retzius cells (CRs) are transient neurons that almost completely disappear in the neocortex after birth but survive up to adulthood in the hippocampus at a certain percentage. CRs are synaptically integrated into hippocampal circuits relating to hippocampal-related behaviors and network. Abnormal survival of CRs leads to deficits in adult neuronal and cognitive functions(16, 17). CRs down-regulate various neural growth and maturation-relevant processes including axon extension (*Sema6d*, *Dclk1*, *Cttn*, *Sin3a*, et al.), dendrite genesis (*Nlgn1*, *Dclk1*, *Farp1*, *Il1rapl1*, et al.), synapse organization (Lrrtm4, Lhfpl4, Farp1, Mark2, et al.) and neuron migration (*Nr4a2*, *Dclk1*, *Sema6a*, *Mark2*, *Cdkl5*). In summary,METH exerts direct neurotoxic effects on NSCs and their development,and indirectly interferes with neurogenesis-assisting cells,resulting in cognitive decline.

Ependymal cells, a type of neuroglia that provides support to neurons, form the epithelial lining of the brain ventricles(18). The influence caused by METH of ependymal cells show enchancement of cilium organization and movement (*Meig1*, *Cfap* family, *Lca5*, *Tmem216*, et al.), and increasing cerebrospinal fluid circulation, which performs response to toxic substance and filtering out harmful molecules. But METH exposure weakens the processes of intracellular transporting (*Ptpn14*, *Pdcd10*, *Txn1*, *Sorl1*, et al.) and protein processing (*Gsn*, *Txn1*, *Tmsb10*, *Sorl1*, et al.) within ependymal cells.

Fibroblasts, derived from embryonic mesenchymal cells, exhibit a wide range of complex and diverse functions in the hippocampus including ECM homeostasis, secretome regulation, mechanosensation, progenitor cell activity, and immune modulation(19). However, their precise roles in this brain region remain poorly understood. In contrast to the saline group, fibroblasts treated with METH demonstrate an enhanced response to metal ions (*Gsn*, *Mt2*, *Mt1*, *Id2*, *Hnrnpa1*) or

toxic subtance (*Gstm1*, *Inmt*, *Mt2*, *Mt1*), as well as inducement of astrocyte differentiation (*Vim*, *Plpp3*, *Sox9*, *Id2*). Notably, JNK or MAPK signaling pathway inhibition (Map4k4, *Sh3rf1*, *Ccn2*, *Gadd45b*, *Dab2*) leads to reduced fibrosis suggesting that fibroblasts may undergo functional transitions from stress responses such as cell death, inflammation, to other functions like cellular support and transformation.

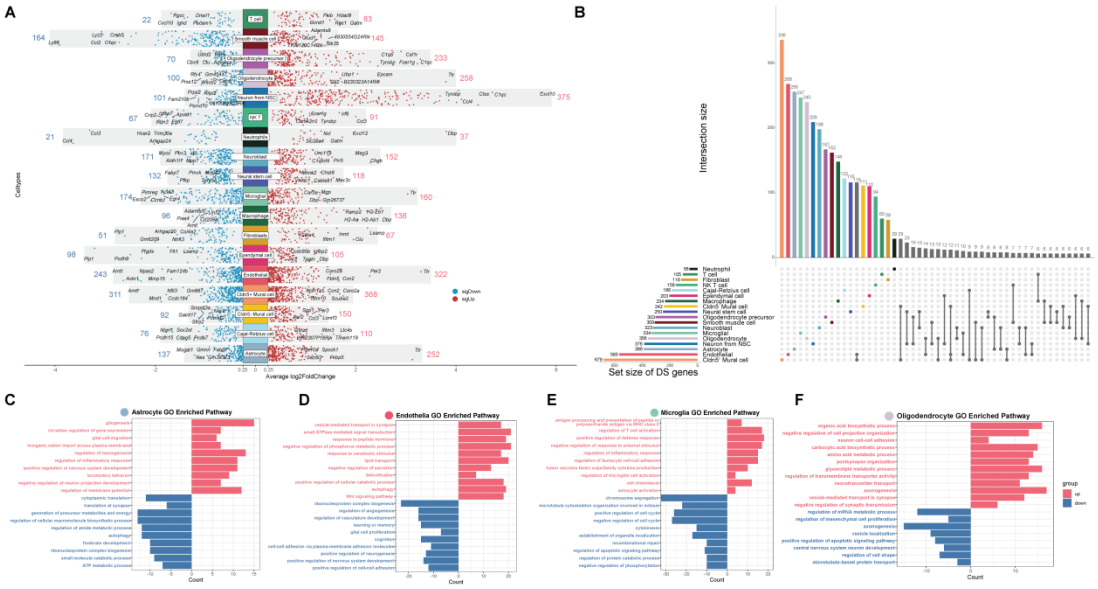

Fig.3. Differentally expressed genes(DEGs) induced by chronic METH exposure in hippocampal cell types. (A) The manhattanplot showing the number of DEGs in each hippocampal cell types(METH v.s. saline), the red dots and number represented for up-regulated genes and the blue ones represented for down-regulated genes. (B) The upset plot showing the number of all of unique and some of shared genes of hippocampal cell types. (C-F) The biocprocess in GO terms enriched separately by up or down-regulated genes of astrocyte, endothelia, microglia and oligodendrocyte. Criteria for DEGs by Muscat: p_value < 0.05, abs(log2FC) > 0.25).

4. METH-induced alterations of crosstalk between cell types in hippocampus led to hippocampal environment disturbance.

Considering the neurotoxic effects of METH on various cell types in the hippocampus and its intricate impact, we conducted an investigation into hippocampal intercellular communication to elucidate the role of these interactions in cognitive decline. Our findings reveal a slight increase in both the total number of cell communication interactions (from 18,396 to 19,054) and their strength (from 0.883 to 0.841) following METH treatment (Fig.4.A). The results demonstrate that chronic METH abuse induces a greater diversity of changes in the differential number of interactions among cell types compared to changes in interaction strength (Fig.4.B and C). For instance, astrocytes mildly enhance the number of interactions with mural cells, ECs, and OPCs but decrease the strength of these interactions, suggesting reduced efficacy of communication signals under METH influence. Neurons from NSC increase the number of interactions with most cell types while exhibiting minimal changes in interaction strength, which corresponds to the upregulation of TNFs and damage signals associated with ER stress or amyloid-beta mentioned in DEGs analysis. In association with neuroinflammatory response, microglia significantly augment their own interaction strength, potentially contributing to neuroinflammation.

From the perspective of cellular communication patterns (incoming and outgoing), hippocampal cells treated with METH exhibit 4 incoming patterns similar to the Saline groups, primarily related to microglial activation, BBB function, neural development, and immunity (Fig.4.D). However, in terms of outgoing patterns, the communication patterns of METH groups are divided into 8 distinct patterns compared to 5 in the Saline group. These outcoming patterns mainly involve microglia activation, endothelial cell signaling, neural development processes, immune responses, as well as a mixed pattern reflecting changes in the neural microenvironment (Fig.4.E). The disruption caused by METH results in confusion within cellular crosstalk specifically through disturbances in outcoming communication pathways within the hippocampus. To further elucidate how METH affects cellular communication networks concretely, we conducted an analysis focusing on specific signal pathway alterations. By calculating Euclidean distance (Fig.4.F), we identified several key differential

functions between METH and Saline groups: RANKL (Receptor Activator of Nuclear Factor-κ B Ligand, belongs to tumor necrosis factor (ligand) superfamily, also proteinically known as TNF-related activation-induced cytokine), SELPLG (proteinically known as p-selectin, involving in leukocyte and microglia activation(20)), and CD46 (proteinically known as complement regulatory protein, as a membrane cofactor mediated cleavage cofactor of C3b and C4b, which is a key regulator of classical and selective complement activation cascade, as well as inflammation(21)). We then compared overall information flow across each signal path to determine conservative and METH-specific signaling pathways (Fig.4.G). Additionally，we also examined changes occurring within each outgoing or incoming signal pathway for individual cell types (Fig.4.H).

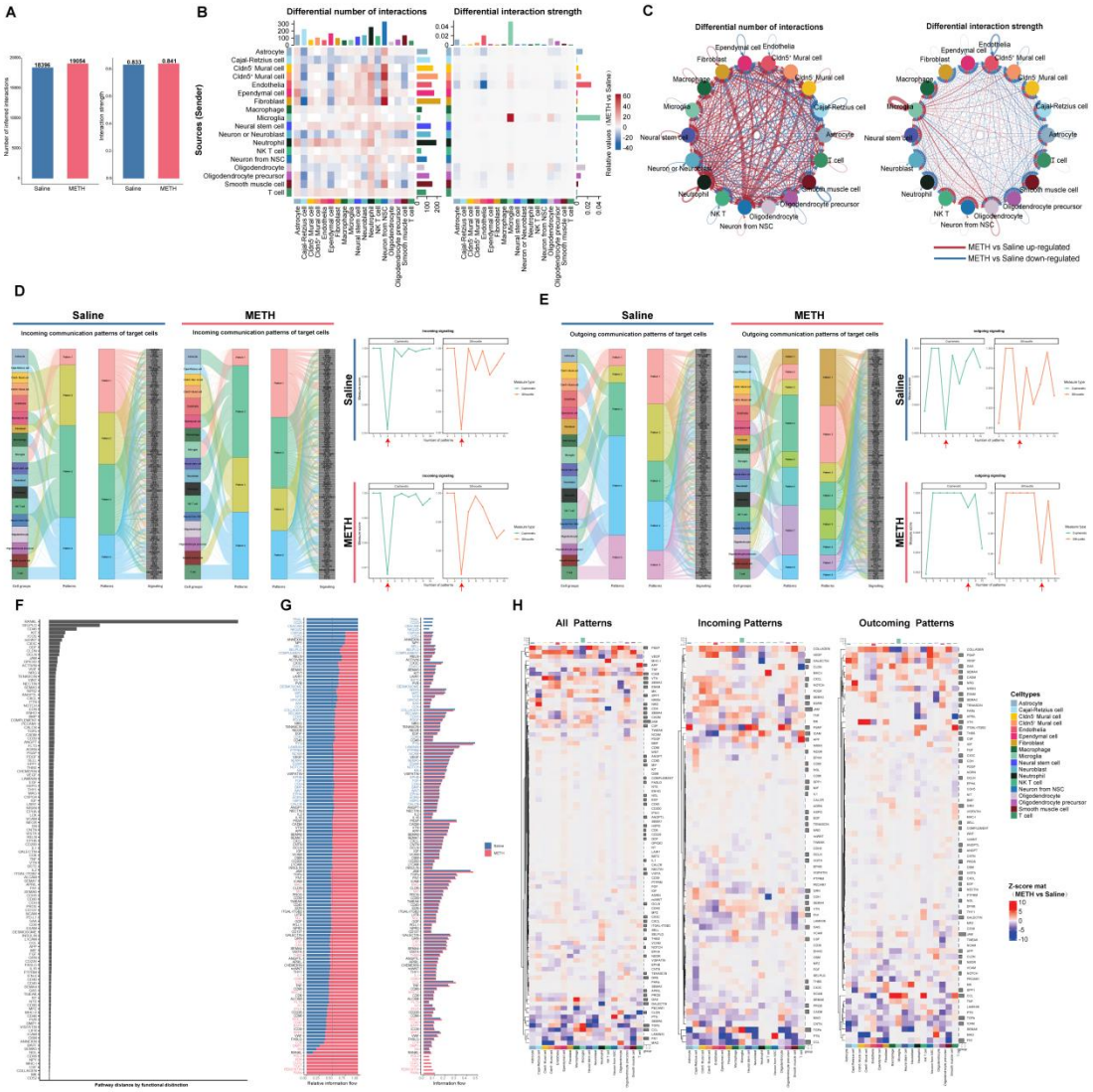

Fig.4. Hippocampal cell types crosstalk alterations induced by chronic METH treatment. (A) The total number of cell communication interactions and the intensity of interactions in saline and METH groups. (B-C) The comparison of the number and the strength of interactions of each cell types between METH and saline groups. (D-E) The incoming and outgoing communication patterns of secreting cells of each groups and the inflection point parameter in clustering algorithm. (F) The identificaton of signaling networks with large (or small) differences according to the Euclidean distance in a shared two-dimensional space. (G) The comparison of the overall information flow of each signal path between two groups. (H) Heatmap showing the incoming, outgoing and all communicated informations' comparison of each signal of each cell type.

5. Pseudo-time series analysis revealed that METH caused changes in hippocampal neurogenesis in mice.

The adult neurogenesis of the dentate gyrus in the hippocampus plays a critical role in cognitive function in mice and is regulated by the local microenvironment. However, there is limited evidence on how METH affects the ability of NSCs to differentiate into neurons, astrocytes, oligodendrocytes, or other cell types. Therefore, we employed pseudotime analysis to investigate the effects of METH chronic exposure on NSC differentiation trends. Along the temporal axis (with NSCs as the starting point), we observed that under normal conditions (Saline group), NSCs (cluster20) exhibited a tendency towards differentiating into neuroblasts (cluster17) more than astrocytes (clusters 6 and 27), following a typical neural development trajectory (Fig.5.A). However, in the METH group, this trajectory was disrupted, indicating a greater likelihood of NSCs differentiating into astrocytes instead of neuroblasts (Fig.5.D), indicating that neurogenesis is hindered. Our analysis reveals that neural development trajectory in METH groups depends on the expression changes of Bsg, Ccl4, Fos, Sox11 (Fig.5.F), as shown by other genes displayed in the heatmap (Fig.5.E); whereas normal developmental progression from NSCs to neuroblasts relies more on Flt1, Hspb1, Igfbp7, Tmsb10 and others (Fig.5.B and C).

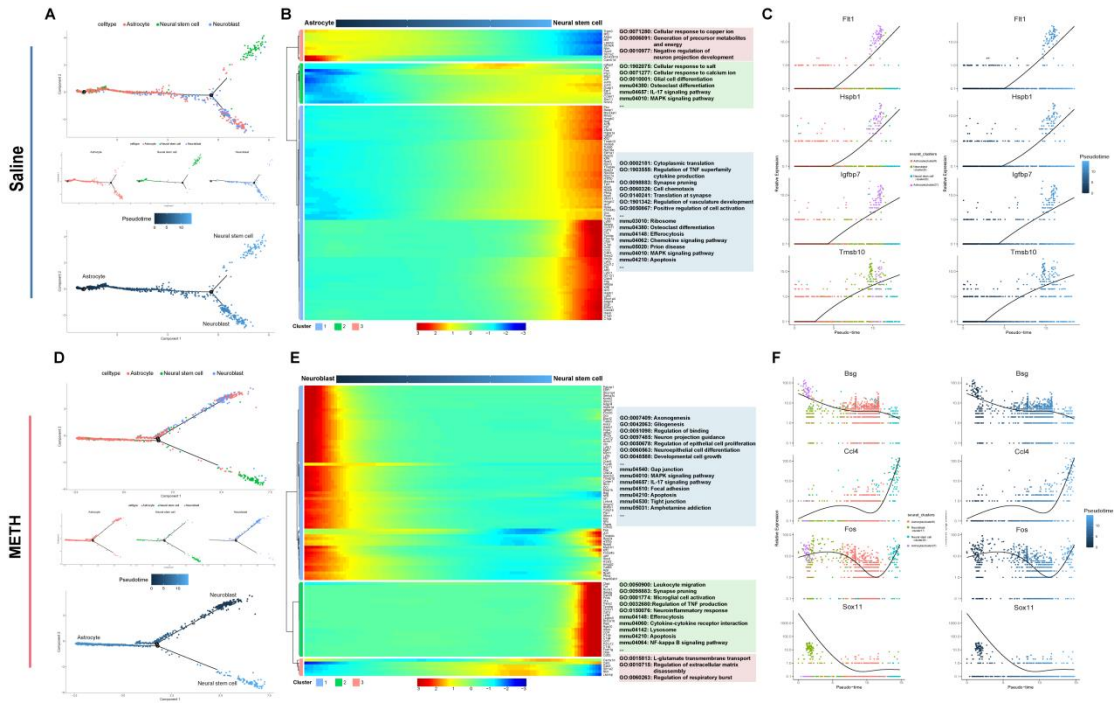

Fig.5. The development direction of hippocampal neural stem cells and the regeneration of hippocampal nerve were analyzed in pseudo-time series. (A, C) The pseudo temporal differentiation locus of neural stem cells, astrocytes and neuroblasts in saline(A) or METH(C) group. (B, D) Heatmap showing the expression of specific genes(rows) in subclusters (columns) along the maturation trajectory from neural stem cells to neuroblasts or astrocytes in saline(B) or METH(D) group, and GO or KEGG funtional enrichment of those genes. (E, F) Pseudotime expression graphs of 4 representative specific marker genes in these cell types showing the development tendency difference in saline(E) or METH(F) group.

6. The change of transcription factor regulatory network is also the cause of cognitive decline caused by METH.

We conducted an analysis of the differential expression of transcription factors in each cell type between METH and Saline mice (Fig.6.A and B). Subsequently, we constructed networks of transcription factor-target genes to predict changes in cellular functions (Fig.6.D-H, SI.3). In astrocytes, a total of 42 differentially expressed transcription factors (DETFs) were identified (Fig.6.C), with their target genes enriched in bioprocesses related to neuron genesis and development, cognition,

inflammatory response regulation, as well as involvement in signaling pathways such as PI3K-Akt, MAPK, cytokine-cytokine receptor interaction et al. (Fig.6.D). Similarly, Endothelial cells exhibite 48 DETFs whose target genes also enrich on neural development bioprocesses including axonogenesis, neuron differentiation and associated with learning or memory. Endothelial cells share same signaling pathways of PI3K-Akt, MAPK as astrocytes (Fig.6.E). Furthermore, the bioprocesses associated with endothelial cells, such as endothelial cell proliferation, cell-cell adhesion, and cell junction assembly, are demonstrated to involve Ras, Focal adhesion, Wnt signaling pathways et al. Despite the presence of only 29 differentially expressed transcription factors (DETFs) in microglia, they exert significant influence on the regulation of membrane potential, axonogenesis and neuron death. These processes are closely linked to synaptic pruning and neuronal survival leading to cognitive dysfunction. Calcium, Wnt, cGMP and cAMP signaling pathways actively participate in these aforementioned biological processes (Fig.6.F). As a supporter of neuronal bodies and axons, oligodendrocytes possess 32 DETFs that regulate the processes of cytoskeletal fibers and axon development, indicating that METH disrupts the transcriptional regulation of neural support genes, rendering neurons more vulnerable to damage. These effects may be mediated through signaling pathways such as Hippo, FoxO, Apelin, and Focal adhesion. Whether the growth of neurons themselves or the maintenance of surrounding cells and environment are disrupted at the transcriptional level under chronic METH treatment, which serves as another reason for the decline of cognitive function in mice. Interestingly, Neuron from NSC and NSC have the most and second most differential TFs, respectively, and share highly similar enrichment terms of target genes related to neurodegenerations such as autophagy or neuron death, axonogenesis, ameboidal-type cell migration and biosynthetic, which is also similar to that of neuroblast (Fig.6.H). This suggests that METH may has common neurotoxic mechanisms on neurons and neural precursor cells by expressing differential neural TFs to regulate similar pathways.

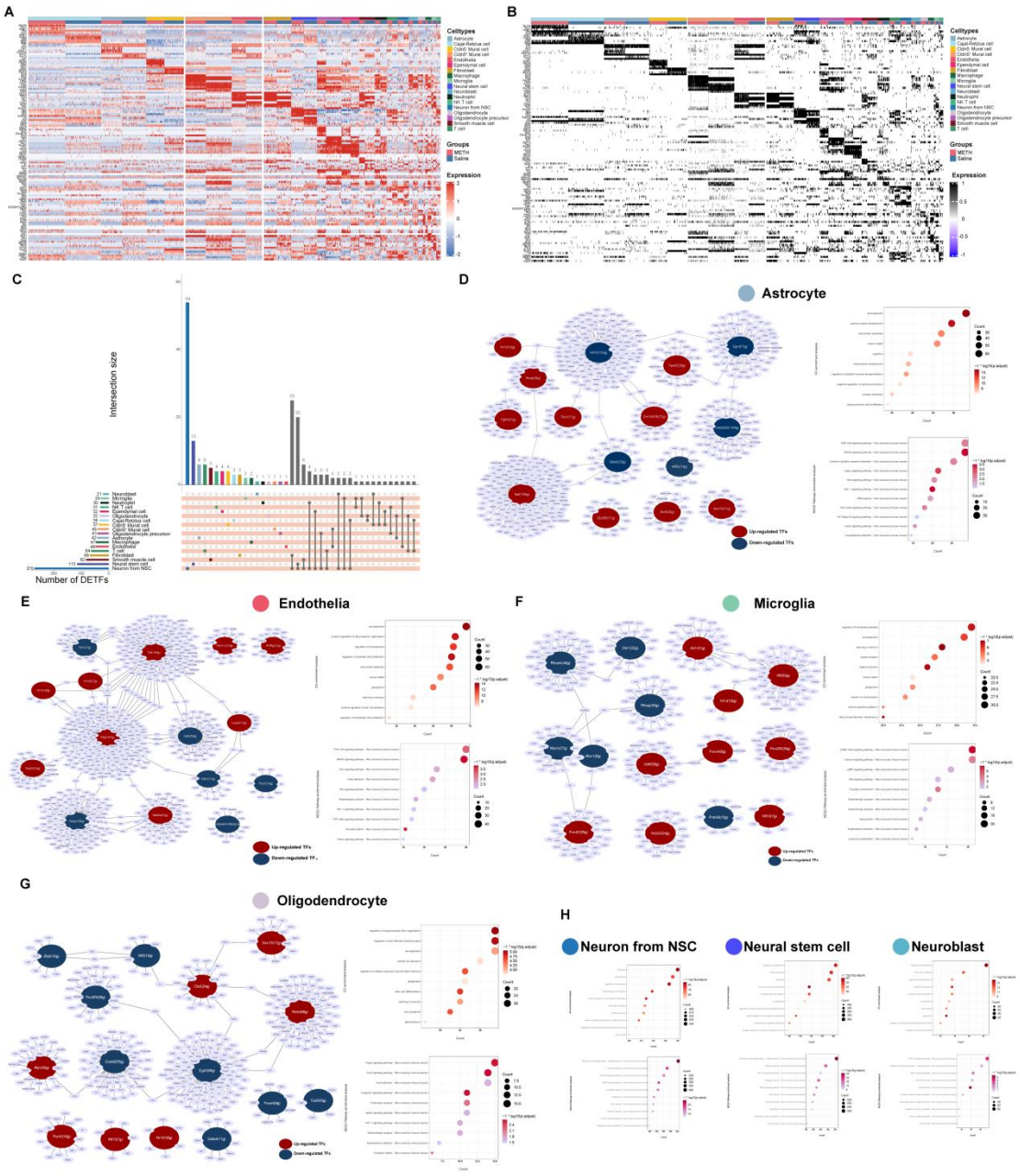

Fig.6. Transcription factor(TF) analysis and function prediction. (A-B) Heatmap of the average expression and the area under the curve (AUC) scores of TF motifs estimated per cell by SCENIC. Shown are top five differentially activated motifs in each cell type of saline and METH groups, respectively. (C) The upset plot showing the number of all of unique and some of shared TFs of hippocampal cell types. (D-G) Gene regulatory network analysis and function enrichment using top 10 of SCENIC identifies critical TFs of astrocytes, endothelia, microglia and oligodendrocytes. (H) Enrichment analysis of target genes predicted by TFs of neuronal development related cell types(Neuron from NSC, NSC and neuroblast).

Discussion

As a psychostimulant drug widely use in worldwide, METH can elevate the risk to various neurological neuropsychiatric disorders due to its addictive and neurotoxic effect. In our study, animal behavior experiments illustrate that chronic METH abuse can cause cognitive decline in mice, which is manifested in spatial cognition, working memory and new object learning. Although previous studies also have similar concusions of METH-induced learning and memory impairments and put forward a variety of therapeutic improvement schemes (e.g. melatonin, oxytocin, housing and tetrahydropalmatine)(22-25), it seems that there are few practical, effective, and recognized treatments for chronic METH abuse-induced cognitive dysfunction therapy. Because researchers have found that METH can affect many organs throughout the body including most areas of the brain by complex and diverse molecular mechanisms, mainly involving excitatory toxicity, neurotransmitter disruption, oxidative stress, cytotoxicity (apoptosis, necrosis, and autophagy), inflammatory response, metabolism disorder et al.. Besides, unlike acute METH injurying, chronic METH abuse is a more complicated process accompanied by the process of toxic injury and repairment.

Hippocampus is essencial for a series of brain advanced functions, such as memory, emotional regulation, and spatial navigation, and its impairment or dysfunction have been proved to closely associate with neuropsychological diseases like neurodegeneration, affective disturbance, and learning disabilities. On the base of our animal behavior results, we used scRNA-seq to investigate all mouse hippocampal cell types except for mature neurons (Due to technical limitation of scRNA-seq, most of mature neurons are lost or destructed during dissociation), in order to explain the heterogeneity of METH effects between different types of cells and provide more targeted mechanisms for METH-induced neurotoxicity and targets for precise therapy.

METH can cause abnormal neuronal function in various direct or indirect ways. METH has a direct toxic effect on neurons causing neuronal damage by various programmed cell death, such as apoptosis, autophagy, necroptosis, pyroptosis, and ferroptosis(26). In spite of mature neurons loss during dissociation, we still isolated the neurons remaining a few NSC markers in some degrees and we considered these neurons developed from NSCs on account of that adult hippocampal neurogenesis is a continuous process. Consistent with previous results, we found a few genes of these neurons related to multiple neuron death biological processes exist differences. For example, Cebpb mediate endoplasmic reticulum stress by Nupr1-C/EBP homologous protein (CHOP) pathway, Prnp/Psenen/apoe are associated with neurodegeneration disease in amyloid-beta metabolic process, Gsk3b increases phosphorylation of Tau, Ddrgk1/Mcl1/Sh3glb1 play important role in mitochondrial autophagy, ATF3 forms dimer with c-Jun to promote apoptosis(27). We also noticed TNFs and ILs overexpression in these neurons may attracts microglia or actives astrocytes leading to neuron death. Abnormal neuronal function is also indirectly related to METH's effects on various auxiliary cells. Our cellchat data showed these neurons generating more communication signals to vascular cells, fibroblasts and ependymal cells after chronice METH treatment. As sources, these neurons upregulate signals like Vegf (Vascular endothelial growth factor, promoting blood vessel growth and increasing permeability.), Sema3b and Sema3c(are critical for neuron projection, guidance of axons, dendritic spine pruning and ECs repulsion(28-30)), Ptn and Mdk (Pleiotrophin and Midkine, as neurotrophic factors, is critical in different steps of differentiation of different cells both in development and in wound repair, especially in neural regeneration, and is up-regulated in drug abuser and neurodegenerative diseases patient(31).), Igf2 (Insulin-like growth factor 2, emerged as a critical molecule of synaptic plasticity and learning and memory(32).), and Cxcl12 (concerning about regulating generation, positioning and maturation of new neurons(33, 34), as well as the communication with blood vessels(35).), but downregulate signals like Bmp6 (Bmp6 level shows an increase in AD-related neurogenic deficits(36), and critical functions to EC differentiation(37).), Bmp7 (Bmp7

expression in radial glial cells may promotes neurogenesis, inhibits gliogenesis(38).), and Fgf2 (a crucial molecule modulating cell proliferation and survival in central nervous system(39).). As receptors, there neurons recept signals from vascular cells mainly about extracellular matrix, such as Col (collagen) families and Lam (laminin) families. Our analysis showed METH impedes the neuronal maturation process which closely relied on the regulation of vascular cells.

METH can cause damage to neurons through various mechanisms, while also have impacts on neural stem/progenitor cells. However, these impacts seem to be different between researches of actue or chronic abuse, intermittent or continuous administration, addiction or withdrawal(40-43). In the researche of chronic METH abuse, it has reported that METH mainly has negetive effects on stem/progenitor cells resulting decreasement proliferative and neurogenesis capacity(40, 44), and even cell death(45, 46). Here our analysis provided in vivo evidences of neurogenesis alterations under chronice METH abuse. We confirmed METH's neurotoxicity to NSCs and progenitor cells like neuroblasts and CRs, and ulteriorly we used pseudotime to explore its influences on differentiation process and dynamics of neural stem cells. The variations of characteristic genes on each branches of neural development trajectory may reveal inflection points in the direction alterations of NSC development under METH effect. It is also necessary to emphsize accurate quantifications of various types of cells counting in the neurogenetic locus will be helpful to lucubrate the toxicity of METH on neurogenesis.

BBB injury is one of neurotoxic mechanisms of METH neurotoxicity, however, the impact of METH on BBB and its consequent effects on neural function far exceed the barrier dysfunction and abnormal substance transport mentioned in current researches. Previous studies of METH neurovascular toxicity have reported that ECs structure and function disorder and astrocytes-released cytokines or damage factors induced injury are parts of proper mechanisms for BBB injury(47), however these studies usually consider a single aspect of cell type or mechanism within BBB while current researches emphasize that NVU comprises more informations about

microcirculation integrity, vascular function and cellular cooperation, which are important to cognition regulation(48). In our study, we parsed most of neurovascular unit (NVU) components which are consisted of ECs, mural cells, SMCs, gial cells(astrocytes, oligodendrocytes and microglia), neurons and basal matrix. We found that ECs can be grouped into several subsets may related to the difference between arteries and veins and the grade of vascular branches, which make it possible to anaylze endothelial dysfunctions like insufficient nutrient and oxygen transport, low clearance efficiency of metabolic waste in cerebral circulation, or leukocyte adhesion and migration. Moreover, mounting evidences correlate mechanical stress with endothelial function, such as barrier function, inflammatory signaling, apoptosis, oxidative stress, endothelial mesenchymal transformation and aging(49), which means ECs located in different fluid states of vascular segments may be regulated variously as results of METH-induced cerebral blood flow abnormalities(50-52). In the meanwhile, the influence of the endothelium on other cell types is extensive, including but not limited to vascular tone or structure, maintenance of collateral vessels, neurotransmission and neurogenesis(48), as our DEGs analysis found that the effects of METH on ECs are not only to damage the junction structure and cause autophagy apoptosis, but also to change the association with other cells, such as GO terms: vesicle-mediated transport in synapse, neurotransmitter transport, or glial cell proliferation. Although there are few METH-induced neurovascular toxicity researches concerning mural cells, who are thought to include pericytes, SMCs and fibroblasts(53), we tried to distinguish them by expression levels of maker genes and eliminate the effect of doublets, and we interestingly found that they share many common genic features as ECs and SMCs, of which some of mural cells have similar expression levels of marker genes as ECs especially. As a result, we classified mural cells as *Cldn5*$^{+}$ and *Cldn5*$^{-}$ mural cells by the similarity to ECs, and we assumed that the diversity of mural cell's functions depends on their proximity and interaction degree to other vascular cells, which is reflecting cellular collaboration in NVU.

Traditional METH research has always linked neuroinflammation to astrocytes, microglia, or certain neuroinflammatory factors, but in recent years, the functions of immune cells residing in neural tissue and the neural immune system deserve our attention. Different neural inflammatory factors or immune signals drive different cellular responses through various signaling pathways. As specialized immune cells of the central nervous system, microglia dominate neuroinflammatory processes under chronice METH exposure and play roles as initiators and executors. We found that microglia in our model up-regulates immune and inflammatory responses, such as MHC class II reaction, IL-1/IL-2/IL-6/TNFs production, and we also noticed that microglia strengthen communications with astrocytes, leukocytes, and lymphocytes whose bioprocesses include activation, differentiation, chemotaxis and migration. It has provided that TNF-α, IL-1α and C1q released by microglia can induce astrocytes to transform into neurotoxic phenotype cells(54). Recent researches pay more attention to the interaction of central and peripheral immune cells influencing neurodegenerations by various mechanisms. Xiaoying Chen et al. reported activate microglia encoding more MHC Ⅰ and Ⅱ proteins recruit T cells into brain parenchyma resulting encephalanalosis(55). Besides, by these innate immune factors, microglia can react to METH-induced DAMPs (damage associated molecular patterns) from neurons or other cells. We also noticed that some of characteristic cellchat signals induced by METH (such as TIGIT, RANKL, SN, SPP1) are mainly caused by these peripheral immune cells espcially NK-T cells. Astrocytes reshape their morphological, genomic, metabolic, and functional characteristics in response to acute or chronic pathological stimuli through a process called reactive astrogliosis(56). Althought we found astrocytes as a whole can regulate inflammatory response, their functions of different subgroups still need to be classfied by genomic and functional features related to their location and interactions with other cells in the CNS. Specially, we noticed second-messenger-mediated signaling-cAMP is up-regulated in astrocytes, and it may act as a molecular switch for neuroprotective astrocyte reactivity(57). A variety of cells and factors in hippucampal microenvironment participate in or influence neuroinflammation after METH exprosure, our data broadened the research

field of neuroinflammation and provided valuable reference genes for various potential inflammatory participants.

The metabolism of various cells effected by METH in the hippocampus can not be ignored, as this may also be the cause or result of changes in cell functions. We have paid particular attention to changes in the metabolism of oligodendrocytes, as it is closely related to the support of neural function and structure.we have found that metabolic processes such as the production of organic acids, amino acids, glycerolipids, and glycolipids occur in oligodendrocytes and are similar to the changes in the expression of lipid transport genes emphasized in AD, which may lead to disruptions in myelin formation or energy supply to neurons(58). Furthermore, endothelial cells and Cldn5+ enterocytes both showed impairments in lipid transport, localization, and metabolism, involving genes such as *Slc2a1*, *Mfsd2a*, *Spp1*, *Apoe*, the *Atp* family, and the *Abca* family. While current research suggests that the characteristics of the BBB in a healthy state are not dependent on the maintenance of microglial cells, the microglial scavenger PLX5622 has been found to impact endothelial cholesterol metabolism(59). Additionally, impaired lipid metabolism in microglial cells is considered an important pathogenic factor in AD(60). So we hypothesize that endothelial and epithelial cell lipid metabolism and transport disorders triggered by METH may promote lipid accumulation in microglia and cause neurological damage.

The disruption of circadian rhythms has rarely been mentioned in previous studies on METH, but METH, as a neurostimulant drug often used in nightlife, can affect sleep. Interestingly, the frequent occurrence of circadian regulation in our analysis of a number of cell-types is also worthy of attention, e.g. Genes involved in circadian rhythm regulation, like *Per2*, *Per3, Ciart*, *Nr1d1* or *Nr1d2,* are up-regulated in gliocytes such as astrocytes, oligodendrocytes and microglia, *Nrd1*, *Nrd2*, *Sfpq* (regulates the circadian clock by repressing the transcriptional activator activity of the CLOCK-ARNTL heterodimer(61)) are up-regulated in macrophage. Recent research had reported that the circadian clock regulates the immune response of various

peripheral innate and adaptive immune cell types and astrocytes and microglia also possess functioning circadian clocks, and circadian timing can affect their inflammatory response, which may be the regulatory mechanism of neuroinflammation in AD(62). Moreover, we noticed that circadian rhythm disorder in endothelia (involving *Per2*, *Cry2*, *Cry1* and *Ptger4*) , smooth muscle cells (involving *Cavin3*, *Kmt2a*, *Per1*, *Nr1d2* et al.) and ependymal cells (involving *Phlpp1*, *Ptgds*, *Clock*, *Id2*). Existing researches showed that the clearance of metabolites, transporter function, permeability, vascular inflammatory and vasomotion of BBB are regulated by circadian rhythm(63-65). A few studies of METH abuse were concerned about circadian rhythm disorder and reported that METH-associated heart failure(66), variability of body temperature(67), Learned motivation(68), addictive properties(69) and learning and memory impairments(23) are affected by disrupted circadian rhythms. However it still needs more researches to figure out the mechanisms of circadian rhythm disturbed by METH and how does circadian rhythm disruption cause METH toxicity.

Conclusion

In conclusion, our reaserch provides scRNA data on the changes of various types of cells in the hippocampus of mice with cognitive impairment caused by METH exposure. These results provide new insights while partially confirming the results of previous studies on METH neurotoxicity. And we will conduct more confirmatory work in the future to elucidate the mechanisms of neurotoxicity and cognitive decline caused by chronic METH abuse.

Ethics approval and consent to participate

All protocols approved by the Institutional Animal Care and Use Committee in Southern Medical University (Ethical number: L2022125), and consistent with NIH Guidelines for the Care and Use of Laboratory Animals (8th Edition, U.S. National Research Council, 2011).

Consent for publication

All authors have approved the manuscript and this submission.

Funding

This work was supported by the Research Projects of National Natural Science Foundation of China (No.82271930) and GuangDong Basic and Applied Basic Research Foundation (2024A1515013050, 2021A1515010909 and 2022A1515110743). The research platforms were supported by Southern Medical University (SMU), Institute of forensic medicine of SMU. We thank Seekgene Biotechnology Co., Ltd for helpful technical support.

Authors and Affiliations

School of Forensic Medicine, Southern Medical University, Guangzhou 510515, Guangdong province, People’ s Republicof China: DF Qiao, H Qiu, X Yue, YB Huang, ZL Meng.

Cancer Research Institute, School of Basic Medical Sciences, Southern Medical University, Guangzhou 510515, China: JH Wang.

Corresponding author: Correspondence to JH Wang and DF Qiao.

Authors' contributions

H Qiu: Conceptualization, Experiments, Data Collection, Statistical Analysis, Sing cell Data Analysis, Writing (Original Draft), Writing (Editing). X Yue, YB Huang and ZL Meng: Animal treatments and Behavior data analysis. JH Wang: Sing-cell Data Analysis, Funding. DF Qiao: Supervision, Funding, Writing (Editing).

Conflict of Interest

The authors declare that they have no known competing financial interests or personal relationships that could have appeared to influence the work reported in this paper.

Availability of data and material

The single-cell RNA-seq data that support findings of this study are available in Gene Expression Omnibus (GEO) under accession numbers GSE252939. Other experimental data and data analysis code can be obtained from the corresponding author at request.

Reference

1. UNODC TUNO.,World Drug Report 2023 (United Nations publication, 2023). www.unodc.org/unodc/en/data-and-analysis/world-drug-report-2023.html., 2023.

2. Thompson PM, Hayashi KM, Simon SL, Geaga JA, Hong MS, Sui Y *et al.*. Structural abnormalities in the brains of human subjects who use methamphetamine. *J NEUROSCI* 2004 2004/6/30; **24**(26)**:** 6028-6036.

3. MacDuffie KE, Brown GG, McKenna BS, Liu TT, Meloy MJ, Tawa B *et al.*. Effects of HIV Infection, methamphetamine dependence and age on cortical thickness, area and volume. *NEUROIMAGE-CLIN* 2018 2018/1/20; **20:** 1044-1052.

4. Schwartz DL, Mitchell AD, Lahna DL, Luber HS, Huckans MS, Mitchell SH *et al.*. Global and local morphometric differences in recently abstinent methamphetamine-dependent individuals. *NEUROIMAGE* 2010 2010/5/1; **50**(4)**:** 1392-1401.

5. Dean AC, Groman SM, Morales AM, London ED. An evaluation of the evidence that methamphetamine abuse causes cognitive decline in humans. *NEUROPSYCHOPHARMACOL* 2013 2013/1/1; **38**(2)**:** 259-274.

6. Guerin AA, Bridson T, Plapp HM, Bedi G. A systematic review and meta-analysis of health, functional, and cognitive outcomes in young people who use methamphetamine. *NEUROSCI*

BIOBEHAV R 2023 2023/10/1; **153:** 105380.

7. Marshall JF, Belcher AM, Feinstein EM, O'Dell SJ. Methamphetamine-induced neural and cognitive changes in rodents. *ADDICTION* 2007 2007/4/1; **102 Suppl 1:** 61-69.

8. Shukla M, Vincent B. Methamphetamine abuse disturbs the dopaminergic system to impair hippocampal-based learning and memory: An overview of animal and human investigations. *NEUROSCI BIOBEHAV R* 2021 2021/12/1; **131:** 541-559.

9. Jin S, Guerrero-Juarez CF, Zhang L, Chang I, Ramos R, Kuan CH *et al.*. Inference and analysis of cell-cell communication using CellChat. *NAT COMMUN* 2021 2021/2/17; **12**(1)**:** 1088.

10. Qiu X, Mao Q, Tang Y, Wang L, Chawla R, Pliner HA *et al.*. Reversed graph embedding resolves complex single-cell trajectories. *NAT METHODS* 2017 2017/10/1; **14**(10)**:** 979-982.

11. Van de Sande B, Flerin C, Davie K, De Waegeneer M, Hulselmans G, Aibar S *et al.*. A scalable SCENIC workflow for single-cell gene regulatory network analysis. *NAT PROTOC* 2020 2020/7/1; **15**(7)**:** 2247-2276.

12. Herrmann C, Van de Sande B, Potier D, Aerts S. i-cisTarget: an integrative genomics method for the prediction of regulatory features and cis-regulatory modules. *NUCLEIC ACIDS RES* 2012 2012/8/1; **40**(15)**:** e114.

13. Li S, Sheng ZH. Oligodendrocyte-derived transcellular signaling regulates axonal energy metabolism. *CURR OPIN NEUROBIOL* 2023 2023/6/1; **80:** 102722.

14. Lezmy J, Arancibia-Carcamo IL, Quintela-Lopez T, Sherman DL, Brophy PJ, Attwell D. Astrocyte Ca(2+)-evoked ATP release regulates myelinated axon excitability and conduction speed. *SCIENCE* 2021 2021/10/15; **374**(6565)**:** eabh2858.

15. Gengatharan A, Malvaut S, Marymonchyk A, Ghareghani M, Snapyan M, Fischer-Sternjak J *et al.*. Adult neural stem cell activation in mice is regulated by the day/night cycle and intracellular calcium dynamics. *CELL* 2021 2021/2/4; **184**(3)**:** 709-722.

16. Riva M, Moriceau S, Morabito A, Dossi E, Sanchez-Bellot C, Azzam P *et al.*. Aberrant survival of hippocampal Cajal-Retzius cells leads to memory deficits, gamma rhythmopathies and susceptibility to seizures in adult mice. *NAT COMMUN* 2023 2023/3/18; **14**(1)**:** 1531.

17. Anstotz M, Lee SK, Maccaferri G. Glutamate released by Cajal-Retzius cells impacts specific hippocampal circuits and behaviors. *CELL REP* 2022 2022/5/17; **39**(7)**:** 110822.

18. Rogers K. "ependymal cell".Encyclopedia Britannica, 5 Dec. 2018.

19. Plikus MV, Wang X, Sinha S, Forte E, Thompson SM, Herzog EL *et al.*. Fibroblasts: Origins, definitions, and functions in health and disease. *CELL* 2021 2021/7/22; **184**(15)**:** 3852-3872.

20. Yeini E, Ofek P, Pozzi S, Albeck N, Ben-Shushan D, Tiram G *et al.*. P-selectin axis plays a key role in microglia immunophenotype and glioblastoma progression. *NAT COMMUN* 2021 2021/3/26; **12**(1)**:** 1912.

21. Cardone J, Le Friec G, Kemper C. CD46 in innate and adaptive immunity: an update. *CLIN EXP IMMUNOL* 2011 2011/6/1; **164**(3)**:** 301-311.

22. Chen YJ, Liu YL, Zhong Q, Yu YF, Su HL, Toque HA *et al.*. Tetrahydropalmatine protects against methamphetamine-induced spatial learning and memory impairment in mice. *NEUROSCI BULL* 2012 2012/6/1; **28**(3)**:** 222-232.

23. Veschsanit N, Yang JL, Ngampramuan S, Viwatpinyo K, Pinyomahakul J, Lwin T *et al.*. Melatonin reverts methamphetamine-induced learning and memory impairments and hippocampal alterations in mice. *LIFE SCI* 2021 2021/1/15; **265:** 118844.

24. Fan XY, Yang JY, Dong YX, Hou Y, Liu S, Wu CF. Oxytocin inhibits methamphetamine-associated learning and memory alterations by regulating DNA methylation at the Synaptophysin promoter. *ADDICT BIOL* 2020 2020/1/1; **25**(1)**:** e12697.

25. Gutierrez A, Jablonski SA, Amos-Kroohs RM, Barnes AC, Williams MT, Vorhees CV. Effects of Housing on Methamphetamine-Induced Neurotoxicity and Spatial Learning and Memory. *ACS CHEM NEUROSCI* 2017 2017/7/19; **8**(7)**:** 1479-1489.

26. Guo D, Huang X, Xiong T, Wang X, Zhang J, Wang Y *et al.*. Molecular mechanisms of programmed cell death in methamphetamine-induced neuronal damage. *FRONT PHARMACOL* 2022 2022/1/20; **13:** 980340.

27. Mei Y, Yuan Z, Song B, Li D, Ma C, Hu C *et al.*. Activating transcription factor 3 up-regulated by c-Jun NH(2)-terminal kinase/c-Jun contributes to apoptosis induced by potassium deprivation in cerebellar granule neurons. *NEUROSCIENCE* 2008 2008/2/6; **151**(3)**:** 771-779.

28. Falk J, Bechara A, Fiore R, Nawabi H, Zhou H, Hoyo-Becerra C *et al.*. Dual functional activity of semaphorin 3B is required for positioning the anterior commissure. *NEURON* 2005 2005/10/6; **48**(1)**:** 63-75.

29. Mohan V, Wade SD, Sullivan CS, Kasten MR, Sweetman C, Stewart R *et al.*. Close Homolog of L1 Regulates Dendritic Spine Density in the Mouse Cerebral Cortex Through Semaphorin 3B. *J NEUROSCI* 2019 2019/8/7; **39**(32)**:** 6233-6250.

30. Martins LF, Brambilla I, Motta A, de Pretis S, Bhat GP, Badaloni A *et al.*. Motor neurons use push-pull signals to direct vascular remodeling critical for their connectivity. *NEURON* 2022 2022/12/21; **110**(24)**:** 4090-4107.

31. Herradon G, Perez-Garcia C. Targeting midkine and pleiotrophin signalling pathways in addiction

and neurodegenerative disorders: recent progress and perspectives. *BRIT J PHARMACOL* 2014 2014/2/1; **171**(4)**:** 837-848.

32. Alberini CM. IGF2 in memory, neurodevelopmental disorders, and neurodegenerative diseases. *TRENDS NEUROSCI* 2023 2023/6/1; **46**(6)**:** 488-502.

33. Trousse F, Jemli A, Silhol M, Garrido E, Crouzier L, Naert G *et al.*. Knockdown of the CXCL12/CXCR7 chemokine pathway results in learning deficits and neural progenitor maturation impairment in mice. *BRAIN BEHAV IMMUN* 2019 2019/8/1; **80:** 697-710.

34. Abe P, Wust HM, Arnold SJ, van de Pavert SA, Stumm R. CXCL12-mediated feedback from granule neurons regulates generation and positioning of new neurons in the dentate gyrus. *GLIA* 2018 2018/8/1; **66**(8)**:** 1566-1576.

35. Li M, Hale JS, Rich JN, Ransohoff RM, Lathia JD. Chemokine CXCL12 in neurodegenerative diseases: an SOS signal for stem cell-based repair. *TRENDS NEUROSCI* 2012 2012/10/1; **35**(10)**:** 619-628.

36. Crews L, Adame A, Patrick C, Delaney A, Pham E, Rockenstein E *et al.*. Increased BMP6 levels in the brains of Alzheimer's disease patients and APP transgenic mice are accompanied by impaired neurogenesis. *J NEUROSCI* 2010 2010/9/15; **30**(37)**:** 12252-12262.

37. Wu X, Yao J, Wang L, Zhang D, Zhang L, Reynolds EX *et al.*. Crosstalk between BMP and Notch Induces Sox2 in Cerebral Endothelial Cells. *CELLS-BASEL* 2019 2019/6/6; **8**(6).

38. Li Z, Liu G, Yang L, Sun M, Zhang Z, Xu Z *et al.*. BMP7 expression in mammalian cortical radial glial cells increases the length of the neurogenic period. *PROTEIN CELL* 2024 2024/1/3; **15**(1)**:** 21-35.

39. Tang MM, Lin WJ, Zhang JT, Zhao YW, Li YC. Exogenous FGF2 reverses depressive-like behaviors and restores the suppressed FGF2-ERK1/2 signaling and the impaired hippocampal

neurogenesis induced by neuroinflammation. *BRAIN BEHAV IMMUN* 2017 2017/11/1; **66:** 322-331.

40. Mandyam CD, Wee S, Crawford EF, Eisch AJ, Richardson HN, Koob GF. Varied access to intravenous methamphetamine self-administration differentially alters adult hippocampal neurogenesis. *BIOL PSYCHIAT* 2008 2008/12/1; **64**(11)**:** 958-965.

41. Recinto P, Samant AR, Chavez G, Kim A, Yuan CJ, Soleiman M *et al.*. Levels of neural progenitors in the hippocampus predict memory impairment and relapse to drug seeking as a function of excessive methamphetamine self-administration. *NEUROPSYCHOPHARMACOL* 2012 2012/4/1; **37**(5)**:** 1275-1287.

42. Galinato MH, Lockner JW, Fannon-Pavlich MJ, Sobieraj JC, Staples MC, Somkuwar SS *et al.*. A synthetic small-molecule Isoxazole-9 protects against methamphetamine relapse. *MOL PSYCHIATR* 2018 2018/3/1; **23**(3)**:** 629-638.

43. Che X, Bai Y, Cai J, Liu Y, Li Y, Yin M *et al.*. Hippocampal neurogenesis interferes with extinction and reinstatement of methamphetamine-associated reward memory in mice. *NEUROPHARMACOLOGY* 2021 2021/9/15; **196:** 108717.

44. Wang S, Wang L, Bu Q, Wei Q, Jiang L, Dai Y *et al.*. Methamphetamine exposure drives cell cycle exit and aberrant differentiation in rat hippocampal-derived neurospheres. *FRONT PHARMACOL* 2023 2023/1/20; **14:** 1242109.

45. Baptista S, Bento AR, Goncalves J, Bernardino L, Summavielle T, Lobo A *et al.*. Neuropeptide Y promotes neurogenesis and protection against methamphetamine-induced toxicity in mouse dentate gyrus-derived neurosphere cultures. *NEUROPHARMACOLOGY* 2012 2012/6/1; **62**(7)**:** 2413-2423.

46. Bento AR, Baptista S, Malva JO, Silva AP, Agasse F. Methamphetamine exerts toxic effects on subventricular zone stem/progenitor cells and inhibits neuronal differentiation. *REJUV RES* 2011 2011/4/1; **14**(2)**:** 205-214.

47. Pang L, Wang Y. Overview of blood-brain barrier dysfunction in methamphetamine abuse. *BIOMED PHARMACOTHER* 2023 2023/5/1; **161:** 114478.

48. Yang Q, Wei X, Deng B, Chang Z, Jin D, Huang Y *et al.*. Cerebral small vessel disease alters neurovascular unit regulation of microcirculation integrity involved in vascular cognitive impairment. *NEUROBIOL DIS* 2022 2022/8/1; **170:** 105750.

49. McQueen A, Warboys CM. Mechanosignalling pathways that regulate endothelial barrier function. *CURR OPIN CELL BIOL* 2023 2023/10/1; **84:** 102213.

50. Li Y, Cui Z, Liao Q, Dong H, Zhang J, Shen W *et al.*. Support vector machine-based multivariate pattern classification of methamphetamine dependence using arterial spin labeling. *ADDICT BIOL* 2019 2019/11/1; **24**(6)**:** 1254-1262.

51. Lafuente JV, Sharma A, Muresanu DF, Ozkizilcik A, Tian ZR, Patnaik R *et al.*. Repeated Forced Swim Exacerbates Methamphetamine-Induced Neurotoxicity: Neuroprotective Effects of Nanowired Delivery of 5-HT3-Receptor Antagonist Ondansetron. *MOL NEUROBIOL* 2018 2018/1/1; **55**(1)**:** 322-334.

52. Ances BM, Vaida F, Cherner M, Yeh MJ, Liang CL, Gardner C *et al.*. HIV and chronic methamphetamine dependence affect cerebral blood flow. *J NEUROIMMUNE PHARM* 2011 2011/9/1; **6**(3)**:** 409-419.

53. Garcia FJ, Sun N, Lee H, Godlewski B, Mathys H, Galani K *et al.*. Single-cell dissection of the human brain vasculature. *NATURE* 2022 2022/3/1; **603**(7903)**:** 893-899.

54. Liddelow SA, Guttenplan KA, Clarke LE, Bennett FC, Bohlen CJ, Schirmer L *et al.*. Neurotoxic reactive astrocytes are induced by activated microglia. *NATURE* 2017 2017/1/26; **541**(7638)**:** 481-487.

55. Chen X, Firulyova M, Manis M, Herz J, Smirnov I, Aladyeva E *et al.*. Microglia-mediated T cell infiltration drives neurodegeneration in tauopathy. *NATURE* 2023 2023/3/1; **615**(7953)**:** 668-677.

56. Lee HG, Lee JH, Flausino LE, Quintana FJ. Neuroinflammation: An astrocyte perspective. *SCI TRANSL MED* 2023 2023/11/8; **15**(721)**:** eadi7828.

57. Cameron EG, Nahmou M, Toth AB, Heo L, Tanasa B, Dalal R *et al.*. A molecular switch for neuroprotective astrocyte reactivity. *NATURE* 2024 2024/2/1; **626**(7999)**:** 574-582.

58. Murdock MH, Tsai LH. Insights into Alzheimer's disease from single-cell genomic approaches. *NAT NEUROSCI* 2023 2023/2/1; **26**(2)**:** 181-195.

59. Profaci CP, Harvey SS, Bajc K, Zhang TZ, Jeffrey DA, Zhang AZ *et al.*. Microglia are not necessary for maintenance of blood-brain barrier properties in health, but PLX5622 alters brain endothelial cholesterol metabolism. *NEURON* 2024 2024/9/4; **112**(17)**:** 2910-2921.

60. Haney MS, Palovics R, Munson CN, Long C, Johansson PK, Yip O *et al.*. APOE4/4 is linked to damaging lipid droplets in Alzheimer's disease microglia. *NATURE* 2024 2024/4/1; **628**(8006)**:** 154-161.

61. Balliu B, Durrant M, Goede O, Abell N, Li X, Liu B *et al.*. Genetic regulation of gene expression and splicing during a 10-year period of human aging. *GENOME BIOL* 2019 2019/11/4; **20**(1)**:** 230.

62. Lananna BV, McKee CA, King MW, Del-Aguila JL, Dimitry JM, Farias F *et al.*. Chi3l1/YKL-40 is controlled by the astrocyte circadian clock and regulates neuroinflammation and Alzheimer's disease pathogenesis. *SCI TRANSL MED* 2020 2020/12/16; **12**(574).

63. He J, Hsuchou H, He Y, Kastin AJ, Wang Y, Pan W. Sleep restriction impairs blood-brain barrier function. *J NEUROSCI* 2014 2014/10/29; **34**(44)**:** 14697-14706.

64. Cuddapah VA, Zhang SL, Sehgal A. Regulation of the Blood-Brain Barrier by Circadian Rhythms

and Sleep. *TRENDS NEUROSCI* 2019 2019/7/1; **42**(7)**:** 500-510.

65. Zhang SL, Lahens NF, Yue Z, Arnold DM, Pakstis PP, Schwarz JE *et al.*. A circadian clock regulates efflux by the blood-brain barrier in mice and human cells. *NAT COMMUN* 2021 2021/1/27; **12**(1)**:** 617.

66. Zhang C, Chen C, Zhao X, Lu J, Zhang M, Qiu H *et al.*. New insight into methamphetamine-associated heart failure revealed by transcriptomic analyses: Circadian rhythm disorder. *TOXICOL APPL PHARM* 2022 2022/9/15; **451:** 116172.

67. Behrouzvaziri A, Zaretskaia MV, Rusyniak DE, Zaretsky DV, Molkov YI. Circadian variability of body temperature responses to methamphetamine. *AM J PHYSIOL-REG I* 2018 2018/1/1; **314**(1)**:** R43-R48.

68. Rawashdeh O, Clough SJ, Hudson RL, Dubocovich ML. Learned motivation drives circadian physiology in the absence of the master circadian clock. *FASEB J* 2017 2017/1/1; **31**(1)**:** 388-399.

69. Sayson LV, Lee HJ, Ortiz DM, Kim M, Custodio R, Lee CH *et al.*. The differential vulnerabilities of Per2 knockout mice to the addictive properties of methamphetamine and cocaine. *PROG NEURO-PSYCHOPH* 2023 2023/8/30; **126:** 110782.

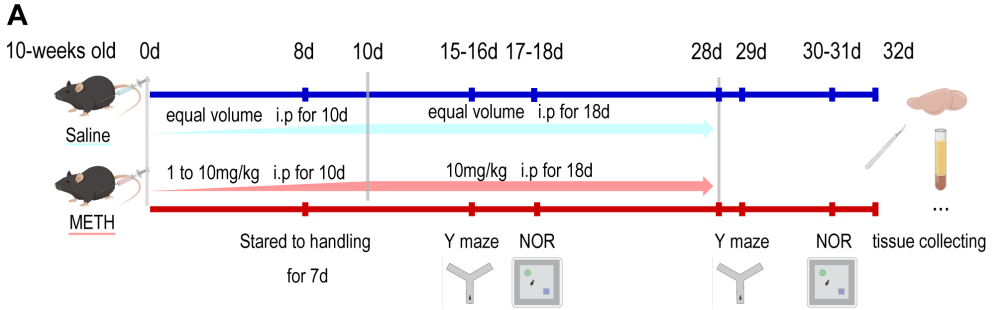
A
10-weeks old
0d
8d
10d
15-16d
17-18d
28d
29d
30-31d
32d
Saline
equal volume i.p for 10d
equal volume i.p for 18d
METH
1 to 10mg/kg i.p for 10d
10mg/kg i.p for 18d
Stared to handling for 7d
Y maze
NOR
Y maze
NOR
tissue collecting

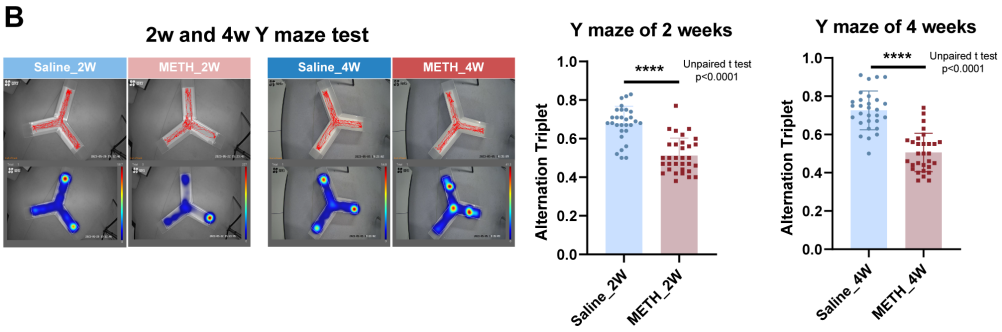
B
2w and 4w Y maze test
Saline_2W
METH_2W
Saline_4W
METH_4W
Y maze of 2 weeks
Y maze of 4 weeks
Alternation Triplet
****
Unpaired t test
p<0.0001
Saline_2W
METH_2W
Saline_4W
METH_4W

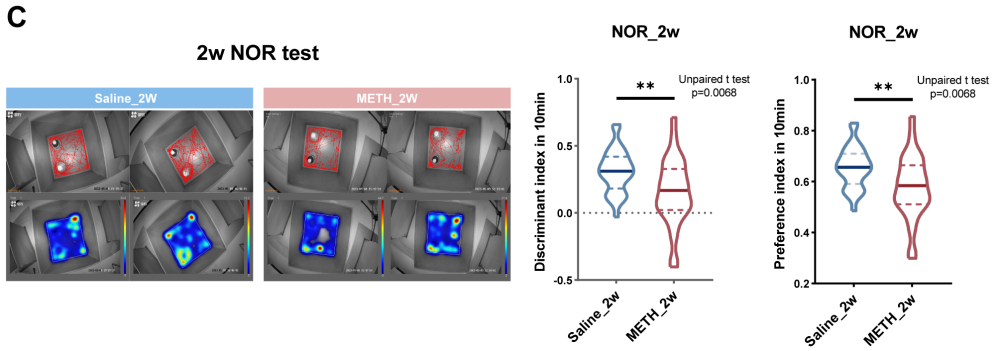
C
2w NOR test
Saline_2W
METH_2W
NOR_2w
Discriminant index in 10min
Preference index in 10min
**
Unpaired t test
p=0.0068
Saline_2w
METH_2w

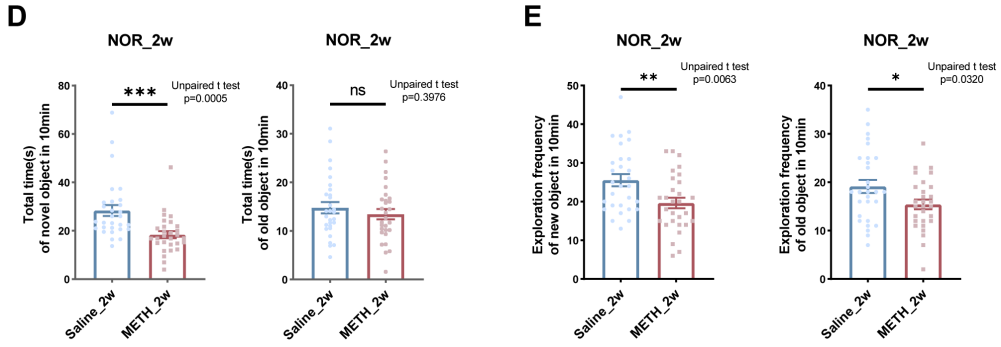
D
NOR_2w
Total time(s) of novel object in 10min
Total time(s) of old object in 10min
***
Unpaired t test
p=0.0005
ns
Unpaired t test
p=0.3976
Saline_2w
METH_2w
E
NOR_2w
Exploration frequency of new object in 10min
Exploration frequency of old object in 10min
**
Unpaired t test
p=0.0063
*
Unpaired t test
p=0.0320

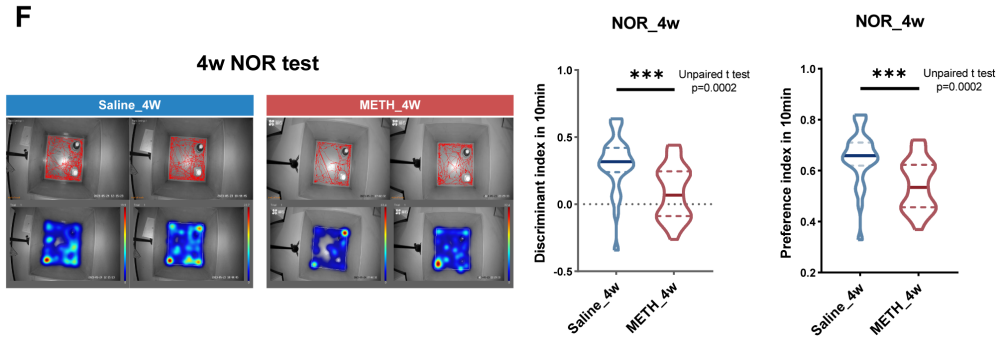
F
4w NOR test
Saline_4W
METH_4W
NOR_4w
Discriminant index in 10min
Preference index in 10min
***
Unpaired t test
p=0.0002
Saline_4w
METH_4w

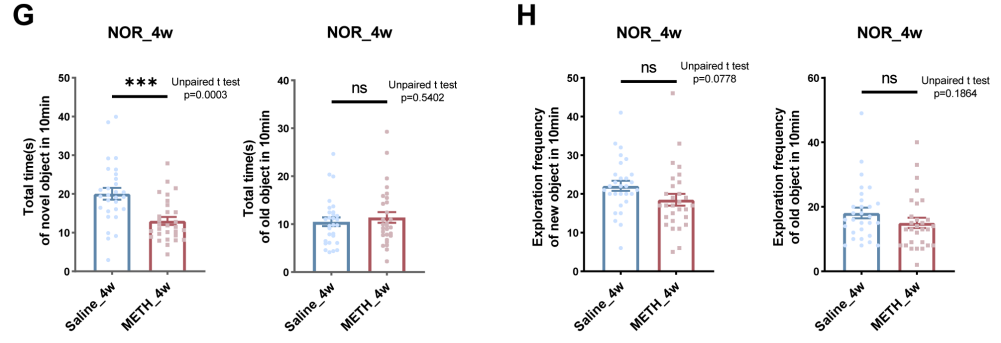
G
NOR_4w
Total time(s) of novel object in 10min
Total time(s) of old object in 10min
***
Unpaired t test
p=0.0003
ns
Unpaired t test
p=0.5402
Saline_4w
METH_4w
H
NOR_4w
Exploration frequency of new object in 10min
Exploration frequency of old object in 10min
ns
Unpaired t test
p=0.0778
ns
Unpaired t test
p=0.1864

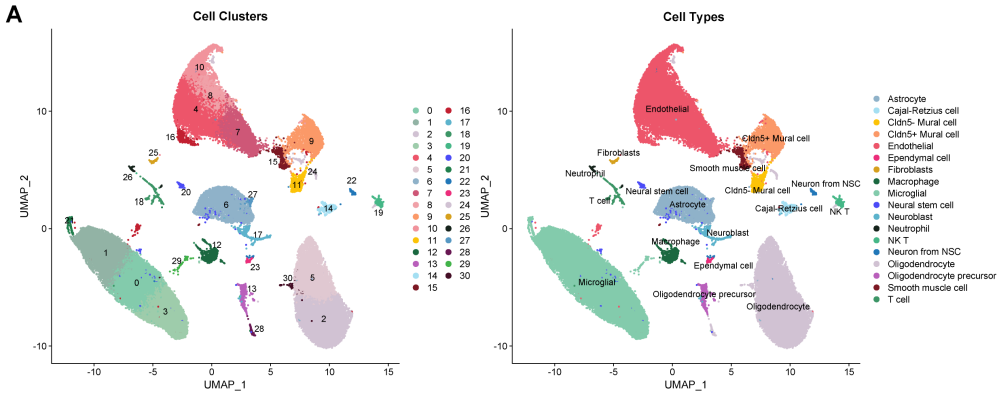

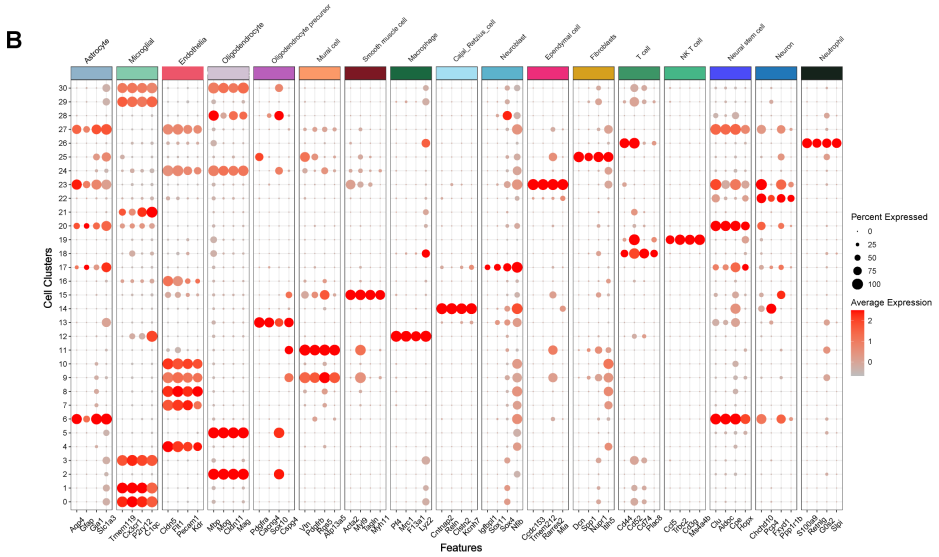

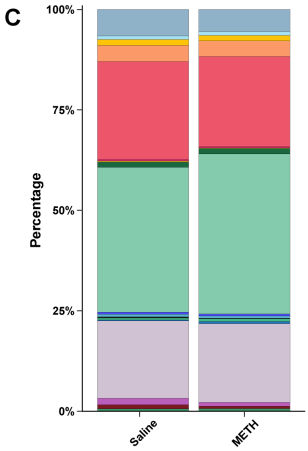

	Percentage of cell types(%)	
	Saline	METH
Astrocyte	6.6	5.5
Cajal−Retzius cell	0.9	1.0
Cldn5− Mural cell	1.5	1.4
Cldn5+ Mural cell	4.1	3.8
Endothelial	24.3	22.5
Ependymal cell	0.4	0.3
Fibroblasts	0.3	0.2
Macrophage	1.3	1.3
Microglial	36.0	39.8
Neural stem cell	0.5	0.5
Neuroblast	0.7	0.6
Neutrophils	0.3	0.1
NK T cell	0.5	0.7
Neuron from NSC	0.2	0.6
Oligodendrocyte	19.3	19.5
Oligodendrocyte precursor	1.6	1.0
Smooth muscle cell	1.0	0.6
T cell	0.5	0.6
Total	100.0	100.0

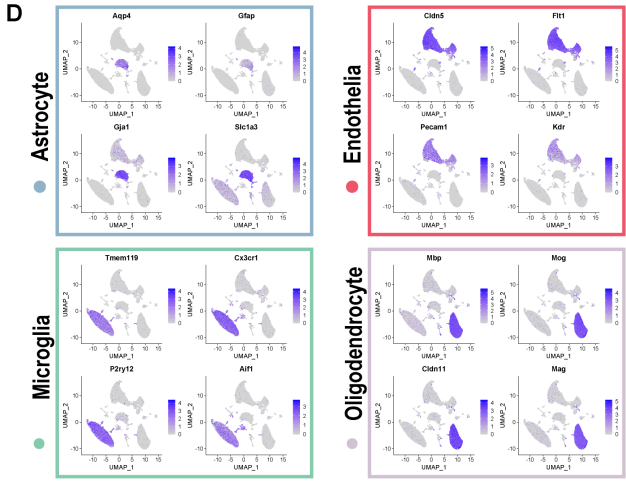

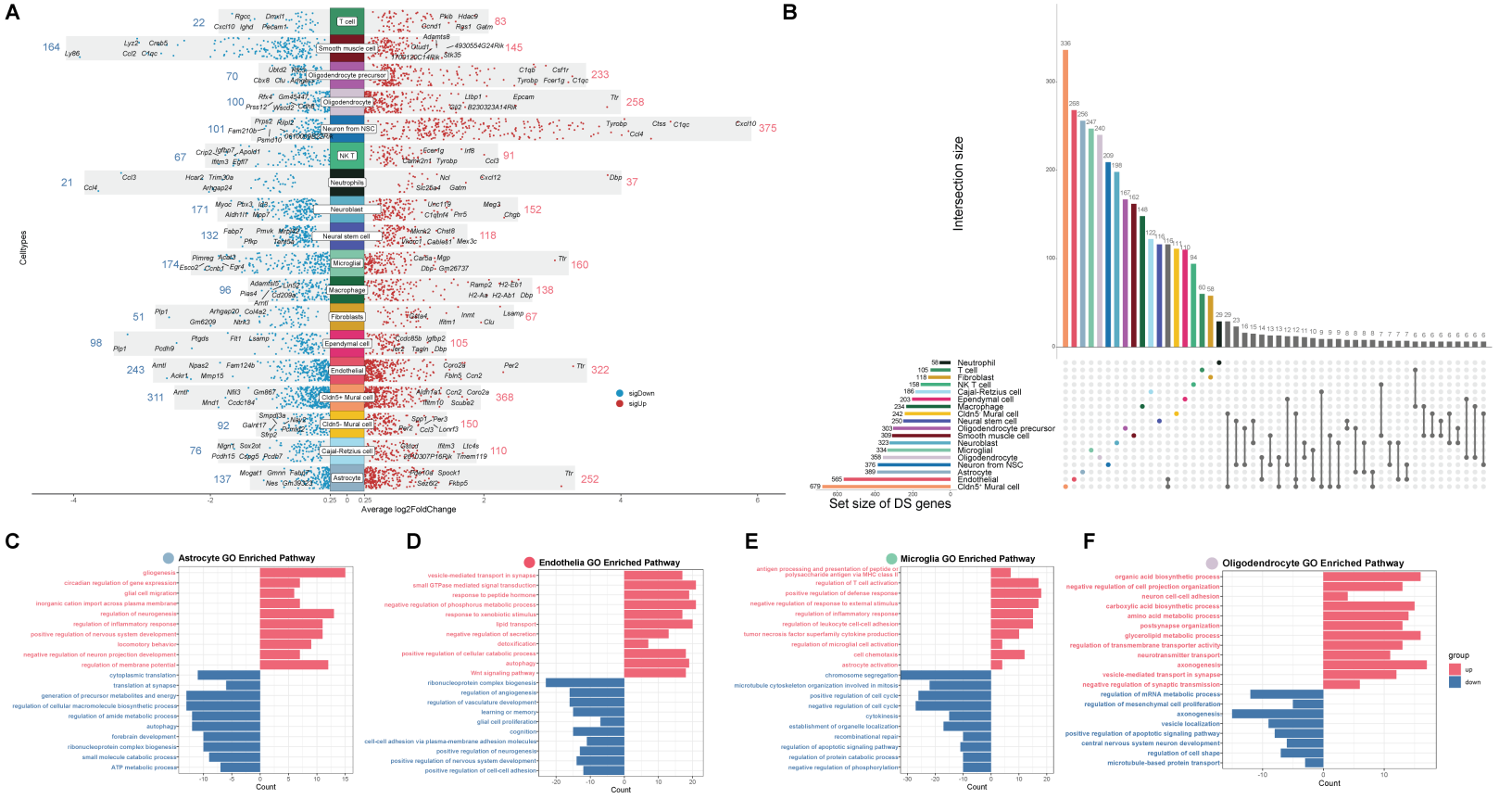
A
Celltypes
Average log2FoldChange
sigDown
sigUp
T cell
Smooth muscle cell
Oligodendrocyte precursor
Oligodendrocyte
Neuron from NSC
NK T
Neutrophils
Neuroblast
Neural stem cell
Microglial
Macrophage
Fibroblasts
Ependymal cell
Endothelial
Cldn5+ Mural cell
Cldn5- Mural cell
Cajal-Retzius cell
Astrocyte
B
Intersection size
Set size of DS genes
Neutrophil
T cell
Fibroblast
NK T cell
Cajal-Retzius cell
Ependymal cell
Macrophage
Cldn5- Mural cell
Neural stem cell
Oligodendrocyte precursor
Smooth muscle cell
Neuroblast
Microglial
Oligodendrocyte
Neuron from NSC
Astrocyte
Endothelial
Cldn5+ Mural cell
C
Astrocyte GO Enriched Pathway
gliogenesis
circadian regulation of gene expression
glial cell migration
inorganic cation import across plasma membrane
regulation of neurogenesis
regulation of inflammatory response
positive regulation of nervous system development
locomotory behavior
negative regulation of neuron projection development
regulation of membrane potential
cytoplasmic translation
translation at synapse
generation of precursor metabolites and energy
regulation of cellular macromolecule biosynthetic process
regulation of amide metabolic process
autophagy
forebrain development
ribonucleoprotein complex biogenesis
small molecule catabolic process
ATP metabolic process
Count
D
Endothelia GO Enriched Pathway
vesicle-mediated transport in synapse
small GTPase mediated signal transduction
response to peptide hormone
negative regulation of phosphorus metabolic process
response to xenobiotic stimulus
lipid transport
negative regulation of secretion
detoxification
positive regulation of cellular catabolic process
autophagy
Wnt signaling pathway
ribonucleoprotein complex biogenesis
regulation of angiogenesis
regulation of vasculature development
learning or memory
glial cell proliferation
cognition
cell-cell adhesion via plasma-membrane adhesion molecules
positive regulation of neurogenesis
positive regulation of nervous system development
positive regulation of cell-cell adhesion
Count
E
Microglia GO Enriched Pathway
antigen processing and presentation of peptide or polysaccharide antigen via MHC class II
regulation of T cell activation
positive regulation of defense response
negative regulation of response to external stimulus
regulation of inflammatory response
regulation of leukocyte cell-cell adhesion
tumor necrosis factor superfamily cytokine production
regulation of microglial cell activation
cell chemotaxis
astrocyte activation
chromosome segregation
microtubule cytoskeleton organization involved in mitosis
positive regulation of cell cycle
negative regulation of cell cycle
cytokinesis
establishment of organelle localization
recombinational repair
regulation of apoptotic signaling pathway
regulation of protein catabolic process
negative regulation of phosphorylation
Count
F
Oligodendrocyte GO Enriched Pathway
organic acid biosynthetic process
negative regulation of cell projection organization
neuron cell-cell adhesion
carboxylic acid biosynthetic process
amino acid metabolic process
postsynapse organization
glycerolipid metabolic process
regulation of transmembrane transporter activity
neurotransmitter transport
axonogenesis
vesicle-mediated transport in synapse
negative regulation of synaptic transmission
regulation of mRNA metabolic process
regulation of mesenchymal cell proliferation
axonogenesis
vesicle localization
positive regulation of apoptotic signaling pathway
central nervous system neuron development
regulation of cell shape
microtubule-based protein transport
Count
group
up
down

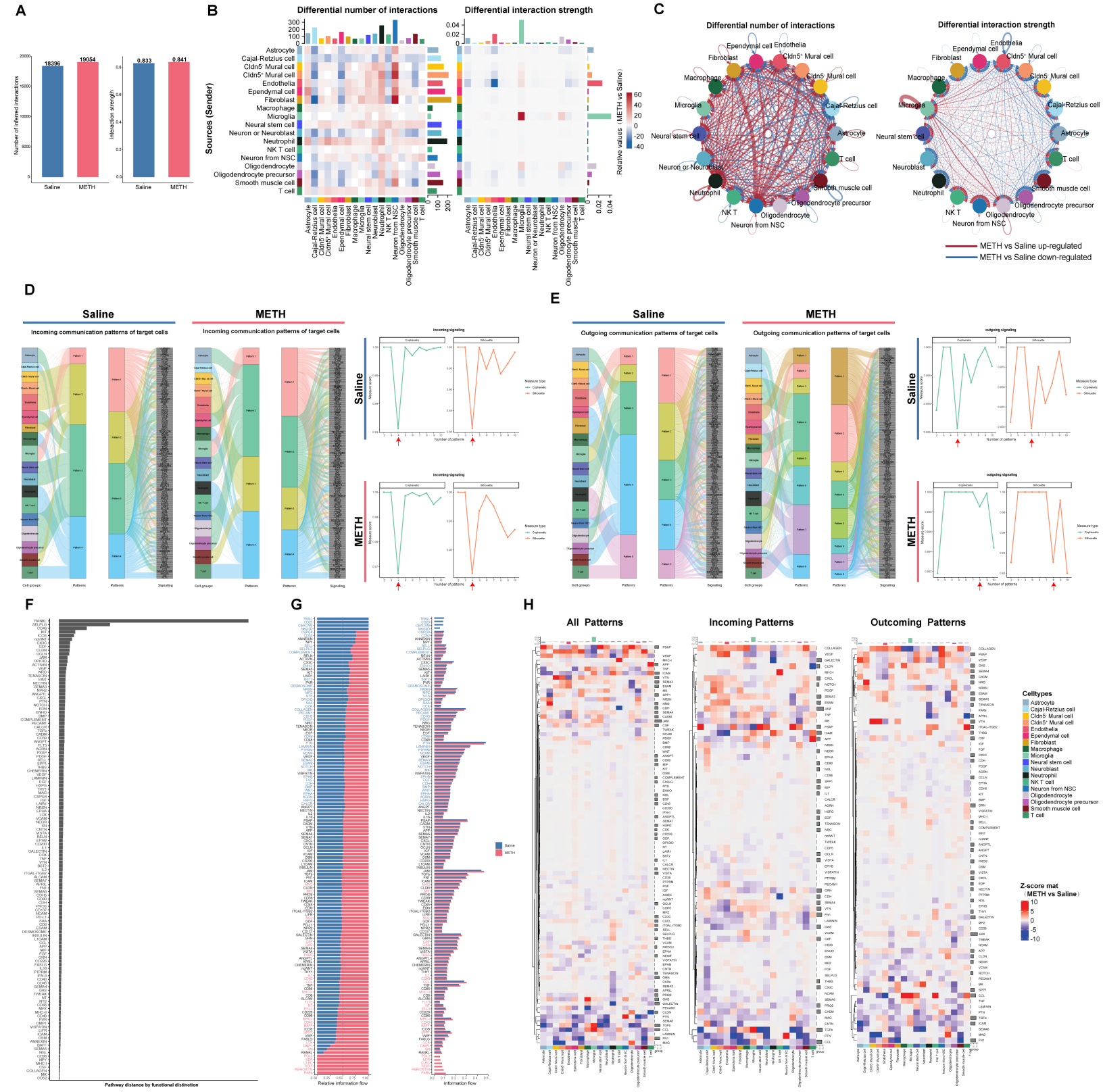
A
18396
19054
0.833
0.841
Number of inferred interactions
Interaction strength
Saline
METH
B
Differential number of interactions
Differential interaction strength
Sources (Sender)
Relative values (METH vs Saline)
Astrocyte
Cajal-Retzius cell
Cldn5⁺ Mural cell
Cldn5⁺ Mural cell
Endothelia
Ependymal cell
Fibroblast
Macrophage
Microglia
Neural stem cell
Neuron or Neuroblast
Neutrophil
NK T cell
Neuron from NSC
Oligodendrocyte
Oligodendrocyte precursor
Smooth muscle cell
T cell
C
Differential number of interactions
Differential interaction strength
METH vs Saline up-regulated
METH vs Saline down-regulated
D
Saline
METH
Incoming communication patterns of target cells
Incoming signaling
Cophenetic
Silhouette
Measure type
Number of patterns
Measure score
Cell groups
Patterns
Signaling
E
Outgoing communication patterns of target cells
outgoing signaling
F
Pathway distance by functional distinction
G
Relative information flow
Information flow
Saline
METH
H
All Patterns
Incoming Patterns
Outcoming Patterns
Celltypes
Astrocyte
Cajal-Retzius cell
Cldn5⁺ Mural cell
Cldn5⁺ Mural cell
Endothelia
Ependymal cell
Fibroblast
Macrophage
Microglia
Neural stem cell
Neuroblast
Neutrophil
NK T cell
Neuron from NSC
Oligodendrocyte
Oligodendrocyte precursor
Smooth muscle cell
T cell
Z-score mat
(METH vs Saline)

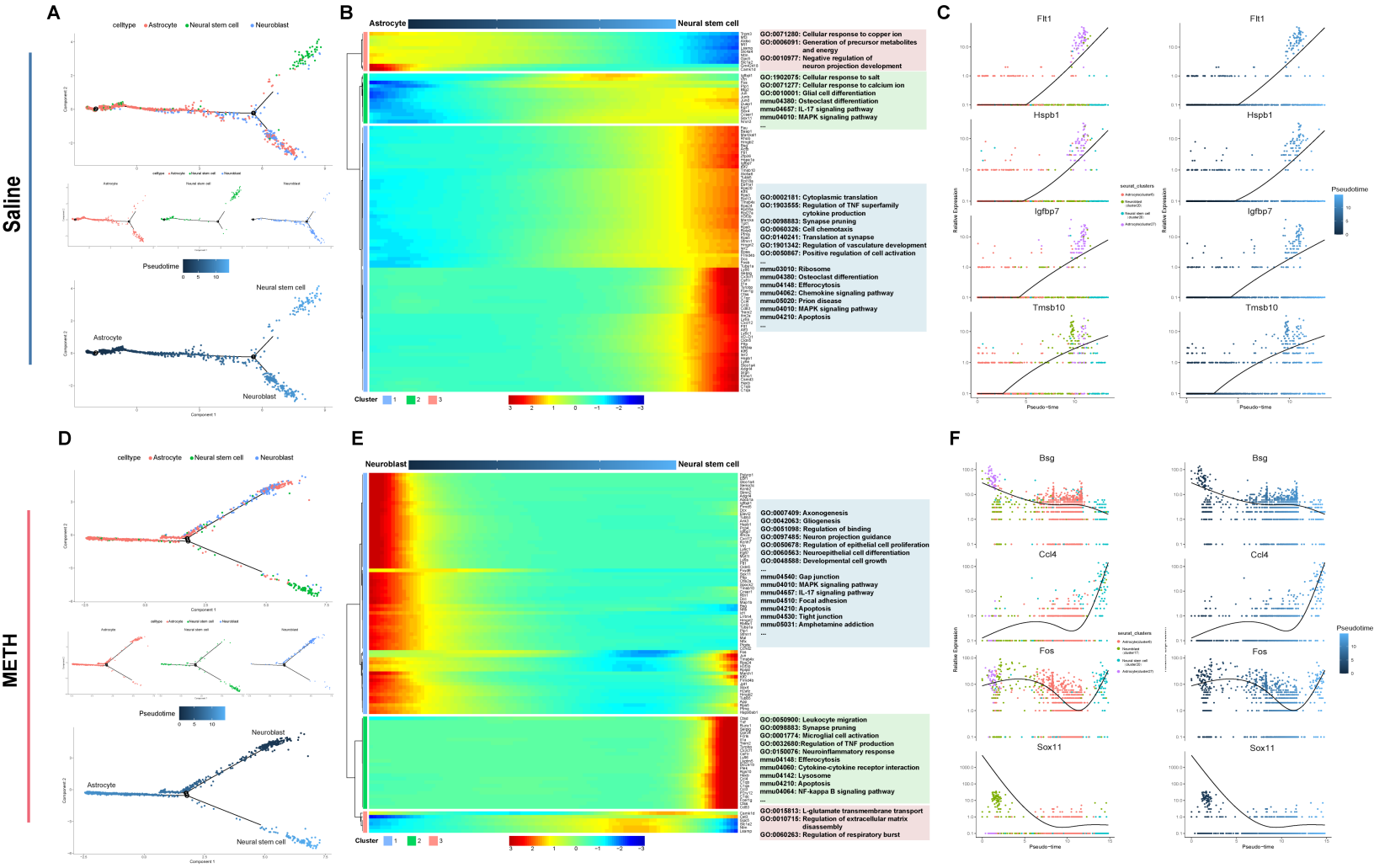
A
B
C
D
E
F
Saline
METH
celltype Astrocyte Neural stem cell Neuroblast
Pseudotime
Neural stem cell
Astrocyte
Neuroblast
Astrocyte Neural stem cell
GO:0071280: Cellular response to copper ion
GO:0006091: Generation of precursor metabolites and energy
GO:0010977: Negative regulation of neuron projection development
GO:1902075: Cellular response to salt
GO:0071277: Cellular response to calcium ion
GO:0010001: Glial cell differentiation
mmu04380: Osteoclast differentiation
mmu04657: IL-17 signaling pathway
mmu04010: MAPK signaling pathway
GO:0002181: Cytoplasmic translation
GO:1903555: Regulation of TNF superfamily cytokine production
GO:0098883: Synapse pruning
GO:0060326: Cell chemotaxis
GO:0140241: Translation at synapse
GO:1901342: Regulation of vasculature development
GO:0050867: Positive regulation of cell activation
mmu03010: Ribosome
mmu04380: Osteoclast differentiation
mmu04148: Efferocytosis
mmu04062: Chemokine signaling pathway
mmu05020: Prion disease
mmu04010: MAPK signaling pathway
mmu04210: Apoptosis
Cluster 1 2 3
Neuroblast Neural stem cell
GO:0007409: Axonogenesis
GO:0042063: Gliogenesis
GO:0051098: Regulation of binding
GO:0097485: Neuron projection guidance
GO:0050678: Regulation of epithelial cell proliferation
GO:0060563: Neuroepithelial cell differentiation
GO:0048588: Developmental cell growth
mmu04540: Gap junction
mmu04010: MAPK signaling pathway
mmu04657: IL-17 signaling pathway
mmu04510: Focal adhesion
mmu04210: Apoptosis
mmu04530: Tight junction
mmu05031: Amphetamine addiction
GO:0050900: Leukocyte migration
GO:0098883: Synapse pruning
GO:0001774: Microglial cell activation
GO:0032680:Regulation of TNF production
GO:0150076: Neuroinflammatory response
mmu04148: Efferocytosis
mmu04060: Cytokine-cytokine receptor interaction
mmu04142: Lysosome
mmu04210: Apoptosis
mmu04064: NF-kappa B signaling pathway
GO:0015813: L-glutamate transmembrane transport
GO:0010715: Regulation of extracellular matrix disassembly
GO:0060263: Regulation of respiratory burst
Flt1
Hspb1
Igfbp7
Tmsb10
Bsg
Ccl4
Fos
Sox11
Relative Expression
Pseudo-time
seurat_clusters
Pseudotime

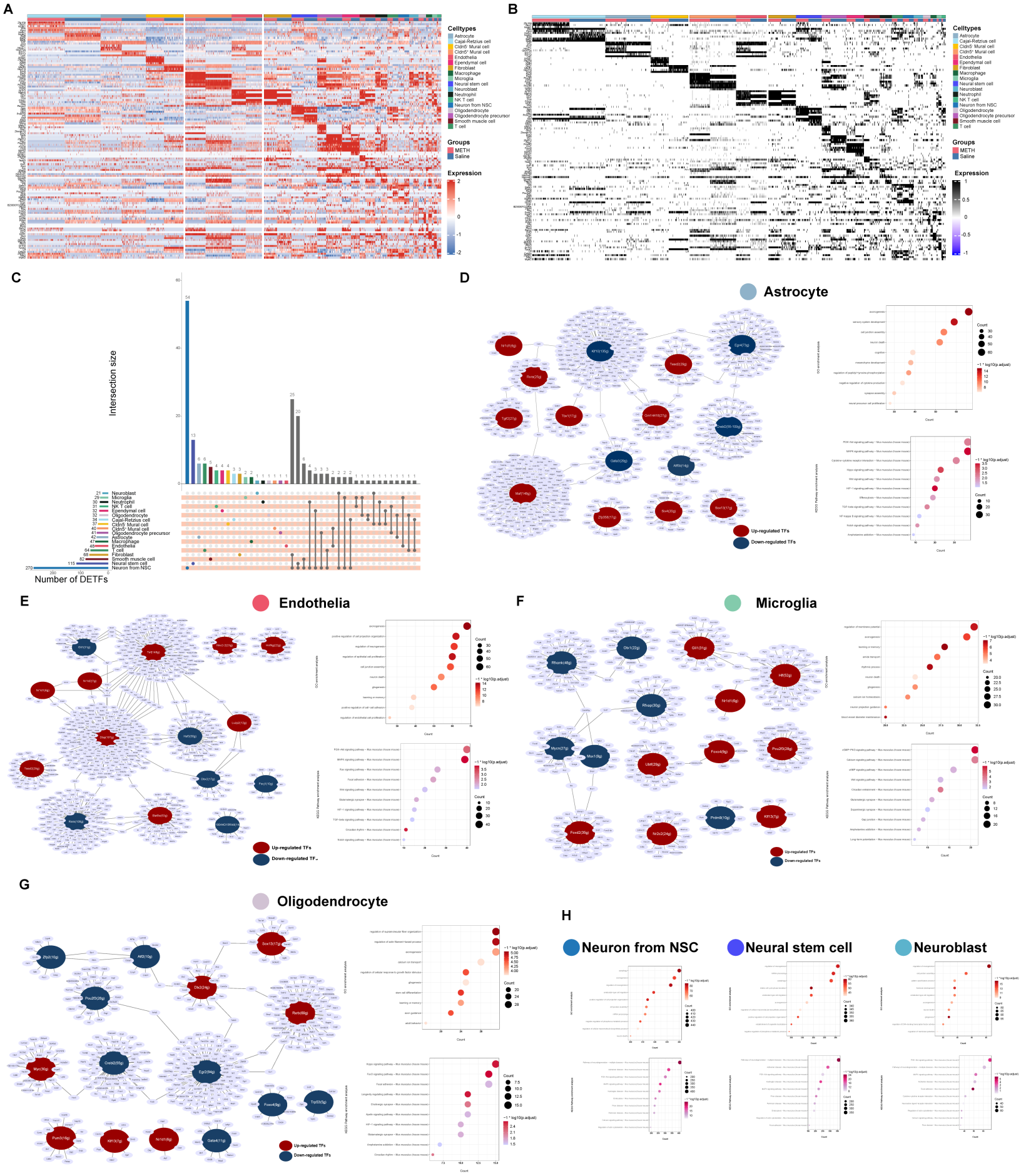
A
B
Celltypes
Astrocyte
Cajal-Retzius cell
Cldn5+ Mural cell
Cldn5- Mural cell
Endothelia
Ependymal cell
Fibroblast
Macrophage
Microglia
Neural stem cell
Neuroblast
Neutrophil
NK T cell
Neuron from NSC
Oligodendrocyte
Oligodendrocyte precursor
Smooth muscle cell
T cell
Groups
METH
Saline
Expression
C
Intersection size
Number of DETFs
D
Astrocyte
Up-regulated TFs
Down-regulated TFs
E
Endothelia
Up-regulated TFs
Down-regulated TFs
F
Microglia
Up-regulated TFs
Down-regulated TFs
G
Oligodendrocyte
Up-regulated TFs
Down-regulated TFs
H
Neuron from NSC
Neural stem cell
Neuroblast